

Inverted regions induced by geometric constraints on a classical encounter-controlled binary reaction

E. Abad*

*Center for Nonlinear Phenomena and Complex Systems,
Université Libre de Bruxelles C.P. 231, 1050 Bruxelles, Belgium*

John J. Kozak

Beckman Institute, California Institute of Technology, Pasadena CA 91125-7400 †

Abstract

The efficiency of an encounter-controlled reaction between two independently-mobile reactants on a lattice is characterized by the mean number $\langle n \rangle$ of steps to reaction. The two reactants are distinguished by their mass with the "light" walker performing a jump to a nearest-neighbor site in each time step, while the "heavy" walker hops only with a probability p ; we associate p with the "temperature" of the system. To account for geometric exclusion effects in the reactive event, two reaction channels are specified for the walkers; irreversible reaction occurs either in a nearest-neighbor collision, or when the two reactants attempt to occupy the same site. Lattices subject to periodic and to confining boundary conditions are considered. For periodic lattices, depending on the initial state, the reaction time either falls off monotonically with p or displays a local minimum with respect to p ; occurrence of the latter signals a regime where the efficiency of the reaction effectively decreases with increasing temperature. Such behavior can also occur when one averages over all initial conditions, but can disappear if the jump probability of the light walker falls below a characteristic threshold value. Even more robust behavior can occur on lattices subject to confining boundary conditions. Depending on the initial conditions, the reaction time as a function of p may increase monotonically, decrease monotonically, display a single maximum or even a maximum and minimum; in the latter case, one can identify distinct regimes where the above-noted inversion in reaction efficiency can occur. We document both numerically and theoretically that these inversion regions are a consequence of a strictly classical interplay between excluded volume effects implicit in the specification of the two reaction channels, and the system's dimensionality and spatial extent. Our results highlight situations where the description of an encounter-controlled reactive event cannot be described by a single, effective diffusion coefficient. We also distinguish between the inversion region identified here and the Marcus inverted region which arises in electron transfer reactions.

PACS numbers: 05.40.-a, 82.20.Fd

Keywords: Diffusion-controlled reactions, lattice walks, first-passage problems

† Permanent address: DePaul University, 243 South Wabash Avenue, Chicago IL 60604-2301

*Corresponding author; Electronic address: eabad@ulb.ac.be

1. INTRODUCTION

Understanding the interplay between diffusion-controlled dynamics and the geometrical constraints imposed by the substrate or topology of the host medium is a problem of seminal importance today. For example, with recent advances in nanotechnology, one can now visualize and manipulate individual atoms and molecules, and design specific geometries on atomic length scales [1, 2, 3]. The geometrical characteristics of the latter (i.e., size, dimensionality and boundary conditions) are found to influence the efficiency of diffusion-controlled reactive processes and trapping events governed by specific interactions.

After the seminal papers by Ovchinnikov and Zeldovich [4] and Toussaint and Wilczek [5] documenting an anomalous decrease in the efficiency of the two-species annihilation reaction in low dimensions due to reactant segregation effects, other types of encounter-controlled processes between unlike species have also received much attention in the literature. In particular, the so-called trapping problem and target problem have been extensively studied [6, 7]. Such processes are ubiquitous in nature and the underlying theory finds wide application in domains such as trapping of charge carriers [8], exciton annihilation and spin relaxation processes [9], quenching of delocalized excitations, recombination and coagulation processes [10], predator-prey models [7, 11] etc. In the simplest version of the trapping problem, diffusing A particles are annihilated upon encounter with immobile traps T following the scheme $A + T \rightarrow T$. The target problem may be thought of as dual to the trapping problem [12, 13], i.e., here randomly moving A particles are the ones which destroy immobile targets T upon encounter according to the reaction $A + T \rightarrow A$. The case where both A particles and traps diffuse with different diffusivities is significantly harder to deal with and few analytic solutions are known [14, 15, 16, 17, 18, 19]. With a few exceptions, most of the previous work on such variants of the trapping and the target problem has been focused on the computation of the survival probability $S(t)$ for the annihilated species and the long-time asymptotics of this property as a measure of the reaction's efficiency.

On the other hand, a number of papers [20, 21, 22] have taken up the problem of characterizing the efficiency of two-particle, encounter-controlled reactions on a lattice. The type of reaction considered in those references can also be interpreted as a space- and time-discrete version of the trapping problem or the target problem as defined above. In contrast to previous work, the quantity used to gauge the efficiency of the process was the initial-condition-averaged mean number of time steps to reaction $\langle n \rangle$, whose inverse is a measure of the time scale of the reaction and hence the efficiency of the reaction-diffusion event; in particular, in the large lattice limit the inverse converges (in magnitude) to the smallest eigenvalue of the associated master equation¹. Basically two types of situations were considered: a) an asynchronous scenario in which a "light" walker (also termed "walker 1" hereafter) performs nearest-neighbor jumps at each time step while a "heavy" walker (walker 2) remains stationary at a given site, thereby playing the role of an immobile trap and b) a situation where both walkers synchronously perform symmetric nearest-neighbor jumps on the lattice. Synchronous dynamics turns out to be more efficient in general, but significant exceptions are found for sufficiently small lattices.

If one assumes, for instance in the framework of Arrhenius theory, that the mobility of the heavy walker grows with increasing system temperature, one realizes that such exceptions

¹ The counterpart $\langle t \rangle$ of $\langle n \rangle$ in the diffusive limit is connected with the survival probability via the relation $\langle t \rangle = \int_0^\infty S(t) dt$, (see e.g. [6], pages 173-174)

are quite remarkable. In classical diffusion theory, as formulated by von Smoluchowski and Einstein, the diffusion coefficient is a monotonically increasing function of the temperature. Thus, in a continuum approximation where one identifies an effective diffusion coefficient the efficiency of an encounter-controlled reaction should increase with increasing temperature. Deviations from this expectation emphasize the fact that some properties (particularly for small systems) are not correctly described by an approach valid for large systems in the thermodynamic limit. It is precisely these properties that are of special importance in applications of nanotechnology.

To understand in a more detailed way the role of temperature in influencing the efficiency of diffusion-controlled events in small systems, the approach taken in [20, 21, 22] was generalized in [23] as follows: a jump probability p of walker was defined such that $p = 0$ corresponded to purely asynchronous behavior and $p = 1$ corresponded to purely synchronous behavior of the two diffusing particles². Interpreting the parameter p as a measure of the “system temperature”, one would intuitively anticipate that an increase in temperature should lead to an increase in the efficiency of reaction. For the model studied in [23] and this paper, this expectation was confirmed for certain initial conditions. However, already in 1D, it was shown that for properly chosen initial conditions the model leads to the onset of a parameter region where $\langle n \rangle$ increases monotonically with p , implying that the efficiency of the reaction decreases with increasing temperature.

In what follows, we shall term this region “inverted” by analogy with the well-known decrease of the reaction rate with increasing temperature predicted by Marcus for electron transfer reactions [24, 25, 26] in certain regimes of parameter space (reaction coordinate, reorganization energy) and later confirmed experimentally [27, 28, 29]. However, we emphasize that our use of this terminology is purely symbolic, since in the cases with which we shall be dealing here the anomalous decrease in efficiency is due to a strictly classical interplay between the system geometry and an “interaction zone” (to be specified in Sec. 2) in binary collisions, rather than a quantum-mechanical analysis of curve crossing between reactant and product states (where Marcus showed that there are regions in which the reaction probability can actually decrease with increase in “driving force” of the reaction). As we shall show, when the size of the “interaction zone” of the two reactants becomes of the same order of magnitude as the system size, anomalous behavior is found.

To explore the relevance of our work to possible experimental realizations, it will be necessary to study in detail the extent to which our “inversion region” is robust with respect to system dimensionality and/or boundary conditions. For example, the difference equation approach developed in [23] for 1D periodic lattices cannot be extended to treat the case of higher dimensions or non-translationally invariant lattices. Accordingly, we apply here the theory of finite Markov processes to investigate the previously-noted, more general cases in detail. Further, we shall consider cases where the jump probability of the “light walker” is restricted to values less than one (and will find that the “inversion region” disappears when the jump probability falls below a threshold value). Finally, we shall propose (several) rationale to explain the quantitative behavior uncovered in our study.

The plan of the paper is then the following: Sec. 2 gives a general definition of the model and shows how in the framework of Markov chain theory the mean reaction time and its

² Note that, even though we have chosen to interpret the difference in the mobility of both walkers for $p < 1$ as a difference in their masses, other interpretations are also legitimate. In nonequilibrium system one could e.g. also speak of a difference in their internal energies.

variance can be extracted from the so-called fundamental matrix (the size of this matrix can be greatly reduced by proper use of the system symmetry). In Sec. 3, we deal with the case of a 1D lattice, thereby comparing the results for the periodic and the confining case. This is done both for specific initial conditions and at a coarse grained level (average over a homogeneous set of initial states). Sec. 4 treats the case of a 2D lattice, both for periodic and confining boundary conditions. Sec. 5 discusses the case where the light walker is allowed to jump with probability less than one at each time step. Sec. 6 gives a physical interpretation of the main results. Finally, Sec. 7 summarizes the conclusions and discusses possible extensions of the model. The appendices A and B contain tables with detailed analytic expressions for the reaction time in the general case treated in Sec. 5.

2. GENERAL FRAMEWORK

2.1. Definition of the model and use of symmetry

Consider two reactants (random walkers labeled, respectively, 1 and 2) performing a time discrete random walk on an N -site lattice with dimensionality and boundary conditions to be specified later. At each time step, walker 1 performs a symmetric nearest-neighbor jump with probability one, while walker 2 either performs a symmetric nearest-neighbor jump with probability p (synchronous step) or remains at the same site (asynchronous step). Any time the walkers jump on the same site or exchange positions by crossing each other, the reaction takes place instantaneously, and the process is terminated. Our main goal will be to clarify how the p -dependence of the mean number of time steps to reaction changes with the boundary conditions and the dimensionality of the system and to elucidate the role of the initial conditions in this context.

The stochastic motion of the two walkers in the above model can be considered as an absorbing Markov chain. In order to characterize the transient states of the chain let us first label the lattice sites from 1 to N . In the case of a 1D lattice this can e.g. be done from left to right (see Fig. 1, left), while in the case of a 2D lattice one can number the lattice sites, say, from left to right and from top to bottom (see Fig. 1, right). We shall consider two types of boundary conditions, i.e. periodic and confining. By confining boundaries (also sometimes termed 'reflecting' in the literature) we mean that whenever either of the two walkers attempts to 'exit' the lattice from a boundary site under the dynamics prescribed above, it is reset to the same position.

Each transient state can thus be expressed by a pair of positive integers x_1 and x_2 representing the instantaneous position of walker 1 and walker 2 in terms of the above lattice site coordinates. Let us hereafter denote by x_1^0 and x_2^0 the initial values of these coordinates. Thus, there are $N(N - 1)$ possible pairs of "non-reactive" initial two-particle configurations (x_1^0, x_2^0) . Each of these configurations has an associated local reaction time $\langle n \rangle_{(x_1^0, x_2^0)}$, whereby the angular brackets denote the average over a uniform ensemble of joint random walk realizations. In addition to these quantities, one can construct an expression for the global reaction time $\langle n \rangle$, i.e., the average over a uniform set of initial conditions (x_1^0, x_2^0) :

$$\langle n \rangle = \frac{1}{N(N-1)} \sum_{\substack{x_2^0=1 \\ x_2^0 \neq x_1^0}}^N \sum_{x_1^0=1}^N \langle n \rangle_{(x_1^0, x_2^0)}. \quad (1)$$

In the present work we shall make an extensive use of symmetry to simplify the calculation of $\langle n \rangle$. Let us e.g. consider the case of a 1D lattice with $N = 4$. The set of initial configurations obtained by assigning different values to x_1^0 and x_2^0 can be represented pictorially as follows:

State (2,1) :	2 - 1 - 0 - 0
State (3,1) :	2 - 0 - 1 - 0
State (4,1) :	2 - 0 - 0 - 1
State (1,2) :	1 - 2 - 0 - 0
State (3,2) :	0 - 2 - 1 - 0
State (4,2) :	0 - 2 - 0 - 1
State (1,3) :	1 - 0 - 2 - 0
State (2,3) :	0 - 1 - 2 - 0
State (4,3) :	0 - 0 - 2 - 1
State (1,4) :	1 - 0 - 0 - 2
State (2,4) :	0 - 1 - 0 - 2
State (3,4) :	0 - 0 - 1 - 2

,where the “1(2)” represent sites occupied by walker 1(2) and the “0” represent empty lattice sites.

In the periodic case, the state of the system is fully characterized by the distance $d = \min(|x_1 - x_2|, N - |x_1 - x_2|)$ between the walkers. Thus, the above 12 states can be lumped into the first 2 states (2,1) and (3,1), respectively numbered as State 1 and State 2 in the short-hand notation to be used in the following.

Let us now consider the case of a confining lattice. In addition to the first two states, one has 4 additional symmetry-distinct states, e.g. (4,1), (3,2), (4,2) and (4,3). In our short-hand notation we thus have:

State 1 :	2 - 1 - 0 - 0
State 2 :	2 - 0 - 1 - 0
State 3 :	2 - 0 - 0 - 1
State 4 :	0 - 2 - 1 - 0
State 5 :	0 - 2 - 0 - 1
State 6 :	0 - 0 - 2 - 1

This numbering procedure for the symmetry-distinct states can now straightforwardly be extended to 1D confining lattices with arbitrary N , i.e. by first setting $x_2 = 1$ and letting x_1 vary from 2 to N , then increasing x_2 by one unit and letting x_1 vary from 3 to N , and so on. One thus obtains $N(N-1)/2$ states characterized by $x_1 > x_2$. In particular, the states for the cases $N = 5$ and $N = 6$ to be dealt with in 3.2 respectively read

State 1 :	2 - 1 - 0 - 0 - 0
State 2 :	2 - 0 - 1 - 0 - 0
State 3 :	2 - 0 - 0 - 1 - 0
State 4 :	2 - 0 - 0 - 0 - 1
State 5 :	0 - 2 - 1 - 0 - 0
State 6 :	0 - 2 - 0 - 1 - 0
State 7 :	0 - 2 - 0 - 0 - 1
State 8 :	0 - 0 - 2 - 1 - 0
State 9 :	0 - 0 - 2 - 0 - 1
State 10 :	0 - 0 - 0 - 2 - 1

and

State 1 :	2 - 1 - 0 - 0 - 0 - 0
State 2 :	2 - 0 - 1 - 0 - 0 - 0
State 3 :	2 - 0 - 0 - 1 - 0 - 0
State 4 :	2 - 0 - 0 - 0 - 1 - 0
State 5 :	2 - 0 - 0 - 0 - 0 - 1
State 6 :	0 - 2 - 1 - 0 - 0 - 0
State 7 :	0 - 2 - 0 - 1 - 0 - 0
State 8 :	0 - 2 - 0 - 0 - 1 - 0
State 9 :	0 - 2 - 0 - 0 - 0 - 1
State 10 :	0 - 0 - 2 - 1 - 0 - 0
State 11 :	0 - 0 - 2 - 0 - 1 - 0
State 12 :	0 - 0 - 2 - 0 - 0 - 1
State 13 :	0 - 0 - 0 - 2 - 1 - 0
State 14 :	0 - 0 - 0 - 2 - 0 - 1
State 15 :	0 - 0 - 0 - 0 - 2 - 1

In the case of a periodic lattice, it is sufficient to consider the first $[N/2]$ states, where $[\cdot]$ is the floor function (largest integer smaller than the argument). In this case, the state number in the short-hand notation is identical with the interparticle distance d .

In order to compute the global reaction time $\langle n \rangle$ from the local ones, one constructs

$$\langle n \rangle = \sum_{i=1}^{N_s} w_i \langle n \rangle_i, \quad (2)$$

where N_s is the number of symmetry distinct states (respectively equal to $[N/2]$ and $N(N-1)/2$ for a periodic and for a confining 1D lattice), $\langle n \rangle_i$ is the reaction time when both walkers start from a given symmetry-distinct initial state i , and w_i are appropriately chosen weights. The latter are easily calculated, e.g. for the periodic 1D lattice one has

$$w_i = \frac{1}{[N/2]} \quad (3)$$

for odd values of N and

$$\begin{aligned}
w_i &= \frac{2}{N-1}, \quad i = 1, \dots, [N/2] - 1, \\
w_{[N/2]} &= \frac{1}{N-1}
\end{aligned} \tag{4}$$

for even values of N . These expressions reflect the fact that for even lattices the statistical weight of the initial condition with maximum distance $[N/2]$ between the walkers is half the weight of the other initial states (which appear twice when taking the average over a homogeneous ensemble of initial conditions), while in the odd lattice case all initial states have the same weight.

2.2. Markovian approach

In the framework of Markov chain theory the mean number of time steps $\langle n \rangle_i$ before termination of a random walk starting from state i is given by the elements of the so-called fundamental matrix. This matrix reads

$$\overline{\overline{\mathbf{N}}} \equiv \sum_{k=0}^{\infty} \overline{\overline{\mathbf{Q}}}^k = (\overline{\overline{\mathbf{I}}} - \overline{\overline{\mathbf{Q}}})^{-1}, \tag{5}$$

where $\overline{\overline{\mathbf{Q}}}$ is the matrix whose elements q_{nm} are the transition probabilities between two transient (non-reactive) states n and m . The matrices $\overline{\overline{\mathbf{Q}}}$ and $\overline{\overline{\mathbf{N}}}$ thus have the dimension $N_s \times N_s$. Denoting by n_{nm} the elements of the fundamental matrix, one then has [30]

$$\langle n \rangle_i = \sum_{j=1}^{N_s} n_{ij}. \tag{6}$$

For small lattices the analytical computation of the transition matrix $\overline{\overline{\mathbf{Q}}}$ in terms of the jump probability p as well as the subsequent derivation of the fundamental matrix is straightforward. The local and the global reaction times are obtained from the matrix elements via eqs. (6) and (2). The variance $\langle v \rangle_i \equiv \langle n^2 \rangle_i - \langle n \rangle_i^2$ can also be extracted from the fundamental matrix. One has [30]

$$\langle v \rangle_i = \left((2\overline{\overline{\mathbf{N}}} - \overline{\overline{\mathbf{I}}})\overline{\overline{\mathbf{T}}} - \overline{\overline{\mathbf{T}}}_{sq} \right)_i, \quad i = 1, \dots, N_s. \tag{7}$$

In this equation, the N_s -dimensional vector $\overline{\overline{\mathbf{T}}}$ is given by

$$\overline{\overline{\mathbf{T}}} = \overline{\overline{\mathbf{N}}} \overline{\overline{\mathbf{\Psi}}}, \tag{8}$$

where $\overline{\overline{\mathbf{\Psi}}}$ is the N_s -dimensional vector with all entries equal to 1. The vector $\overline{\overline{\mathbf{T}}}_{sq}$ is obtained from $\overline{\overline{\mathbf{T}}}$ by squaring all entries. The average $\langle v \rangle$ over the initial conditions is obtained by evaluating the weighted sum

$$\langle v \rangle = \sum_{i=1}^{N_s} w_i \langle v \rangle_i. \tag{9}$$

3. 1D LATTICE

3.1. Periodic boundary conditions

The Markov method can be used to recover results reported earlier [23] using an approach based on backward difference equations. The first (rather remarkable) result obtained at this level is that the local reaction times $\langle n \rangle_i$ (where the subscript i is by construction equal to the initial interparticle distance d^0) do not always decay monotonically with the mobility p , as one might expect from an analysis of the relative motion of the two walkers using a continuum approach. Indeed, monotonic decay of the $\langle n \rangle_i$'s only takes place for even values of i , whereas for odd values a local minimum is observed (see Fig. 2). This minimum shifts to higher p values with increasing initial interparticle distance $d^0 \equiv i$. The existence of such a minimum means that there is an anomalous inverted region in which $\frac{d\langle n \rangle_i}{dp} > 0$, implying that the efficiency of the reaction decreases with increasing temperature. Even though this behavior holds both for even and odd values of N the minima are rather shallow in the odd lattice case and are therefore lost when one takes the average over the initial conditions to compute $\langle n \rangle$, in contrast to the even lattice case. Indeed, in computing $\langle n \rangle$ as a function of p via eq. (2), one finds that $\langle n \rangle$ the behavior is different for even and odd lattices, i.e., $\langle n \rangle$ decays monotonically for odd values of N , while for even values a minimum of $\langle n \rangle$ for an intermediate value $p = p_{min}^{(n)}$ is observed ³ (see Fig. 3 and Table 1 for the detailed analytic expressions of $\langle n \rangle$ as a function of p). In other words, for $p > p_{min}^{(n)}$ one again observes an inverted region where $\frac{d\langle n \rangle}{dp} > 0$. The value of $p_{min}^{(n)}$ is strongly size-dependent and shifts to the right as N becomes large, i.e., $\lim_{N \rightarrow \infty} p_{min}^{(n)} = 1$ (see Table 2).

A qualitative explanation for the existence of a minimum in the case of an even lattice has been given elsewhere [31]. This argument suggests that for lattices with an even number of sites the number of statistical paths leading to prereactive configurations with both particles at nearest neighbor sites is larger than in the odd lattice case. In such a prereactive state, the next step will lead to instantaneous reaction with a higher probability if it is asynchronous. A small degree of asynchronicity may thus diminish the probability of mutual avoidance within the typical interaction zone and thereby result in an increase of the reaction rate with respect to the fully synchronous case $p = 1$. The maximum efficiency will therefore correspond to a mixture of synchronous and asynchronous steps. This effect is expected to wash out with increasing lattice size, since “diffusional” transport over long distances then becomes the rate limiting step, and the latter is optimized by purely synchronous transport. Note also that a very similar argument may be invoked to explain the shift of the minimum towards larger p -values observed in the curves $\langle n \rangle_i(p)$ with increasing initial separation i .

These results can be straightforwardly extended to higher-order moments. In the 1D case, this is most naturally done via a generating function approach [32, 33], but the computation of the second-order moment is also possible in the framework of Markov theory (cf. eqs. (7) and (9)). Remarkably, the variances $\langle v \rangle_i$ and $\langle v \rangle$ behave in a similar way as the first order moments. For example, the global variance $\langle v \rangle$ decreases monotonically with p for odd lattices, whereas for even values of N the curves $\langle v \rangle(p)$ display a minimum at a value $p = p_{min}^{(v)}$ which again rapidly shifts towards one with increasing lattice size (see Tables 3

³ This has been verified for lattice sizes up to $N=36$.

and 4 and Fig. 4). One has $p_{min}^{\langle v \rangle} < p_{min}^{\langle n \rangle}$ with the exception of the $N = 4$ lattice, for which both probabilities are equal (compare Tables 2 and 4). Thus, the quantities $\langle v \rangle$ and $\langle n \rangle$ cannot be minimized simultaneously in general.

In the limiting cases $p = 0$ (where the heavy walker plays the role of a stationary trap) and $p = 1$ (limit of identical walkers), it is possible to recover previous results valid for arbitrary lattice size N . In the framework of the Markov approach, these expressions for the reaction time and its variance can be constructed by identifying patterns in the (integer) values generated in calculating these quantities as a function of increasing N . In particular, one has

$$\langle n \rangle_i = i(N - i) \quad (10)$$

in the $p = 0$ case [32] and

$$\langle n \rangle_i = -\frac{i^2}{2} + \frac{Ni}{2} + \frac{1}{4}(1 - (-1)^N)(-1)^i i + \frac{1}{4} \left(N + \frac{(-1)^N + 1}{2} \right) (1 - (-1)^i) \quad (11)$$

in the $p = 1$ case, whereby i can in both cases take any possible values of the initial interparticle distance d^0 , i.e. $i = 1, 2, \dots, [N/2]$.

Note that when N and i take even values, one has $\langle n \rangle_i = i(N - i)/2$, implying that the reaction time takes half the value of the $p = 0$ case, as one would expect from the result obtained in the continuum limit. If one now considers the average over a uniform ensemble of non-reactive configurations one respectively has

$$\langle n \rangle = \sum_{i=1}^{[N/2]} w_i \langle n \rangle_i = \frac{N(N + 1)}{6} \quad (12)$$

for $p = 0$ [32, 34] and

$$\begin{aligned} \langle n \rangle &= N(N + 1)(N + 2)/(12(N - 1)) && N \text{ even,} \\ &= (N + 1)(N + 3)/12 && N \text{ odd} \end{aligned} \quad (13)$$

for $p = 1$. According to Eqs. (12) and (13) the purely synchronous case ($p = 1$) is more effective than the purely asynchronous case ($p = 0$) for all lattices with $N \geq 3$, as one would anticipate from the continuum approximation.

Turning now to the variance, one has

$$\langle n^2 \rangle_i - \langle n \rangle_i^2 = \frac{i^4}{3} - \frac{2N}{3}i^3 + \frac{2}{3}i^2 + \frac{N(N^2 - 2)}{3}i - i^2(N - i)^2 \quad (14)$$

and

$$\langle v \rangle = \frac{N(N + 1)(N - 2)(N + 2)}{30}. \quad (15)$$

when $p = 0$. In the $p = 1$ case the local variance is given by

$$\begin{aligned} \langle n^2 \rangle_i &= \frac{1}{12}i^4 - \frac{1}{6}Ni^3 + \left(\frac{1}{6} - \frac{1}{4}(N+1)(1 - (-1)^i)\right)i^2 + \left(\frac{1}{12}N^3 + \frac{1}{12}N + \frac{1}{4}N^2\right)i + \frac{1}{8} + \frac{1}{3}N \\ &\quad + \frac{1}{24}N^3 + \frac{1}{4}N^2 - \left(\frac{1}{8} + \frac{1}{3}N + \frac{1}{24}N^3 + \frac{1}{4}N^2\right)(-1)^i - \frac{1}{4}(N+1)Ni(-1)^i \end{aligned} \quad (16)$$

for even values of N and

$$\begin{aligned} \langle n^2 \rangle_i &= \frac{1}{12}i^4 - \frac{1}{6}(N + (-1)^i)i^3 + \left(\frac{1}{6} - \frac{1}{4}N(1 - (-1)^i)\right)i^2 + \left(\frac{1}{12}N^3 + \frac{1}{4}N^2 - \frac{1}{6}N\right)i \\ &\quad - \frac{1}{24}N + \frac{1}{24}N^3 + \frac{1}{8}N^2 + \left(\frac{1}{24}N - \frac{1}{24}N^3 - \frac{1}{8}N^2\right)(-1)^i + \left(\frac{1}{4}N - \frac{1}{12}\right)i(-1)^i \end{aligned} \quad (17)$$

for odd values of N . Thus, the global variance becomes

$$\langle v \rangle = \begin{cases} N(N+1)(N+2)(N^2+2N+2)/(120(N-1)) & \text{for } N \text{ even,} \\ (N+1)(N+3)(N^2+2N-5)/120 & \text{for } N \text{ odd.} \end{cases} \quad (18)$$

3.2. Confining boundary conditions

We now consider the behavior of a 1D system subject to confining boundary conditions, and compare this with the behavior summarized above for periodic boundary conditions. The differences can already be seen by examining the three simplest cases: $N = 4$, $N = 5$ and $N = 6$.

In the $N = 4$ case there are 6-symmetry distinct initial states in the $N = 4$ case, as already seen in 2.1. The initial states 1, 2 and 3 correspond to configurations with walker 2 at a boundary site. In all three cases, the associated reaction times are found to decay monotonically with p . In contrast, the $\langle n \rangle_i(p)$ plots for the initial conditions 4, 5 and 6 display at least one inverted region where $\frac{d\langle n \rangle_i}{dp} > 0$ (see Fig. 5). The behavior for initial condition 4 is rather complex, i.e., the reaction time displays a maximum for small values of p and a minimum for large values of p , thereby giving rise to a double inverted region, as shown in the inset of Fig. 5. On the other hand, $\langle n \rangle_5$ rapidly reaches a maximum for small values of p and then decays sharply with p . Finally, $\langle n \rangle_6$ increases monotonically for all p , i.e., the inverted region comprises the whole p -interval. We thus see that the behavior of the efficiency in the confining case is far more complex than in the periodic case, where only monotonically decreasing curves or curves with a single minimum are observed.

In the cases $N = 5, 6$ a similar qualitative behavior is observed. More specifically, the initial states 1 to $N - 1$ correspond to monotonically decreasing reaction times, while the initial states N to N_s are associated with $\langle n \rangle_i(p)$ curves displaying inverted regions with positive p -derivative. In some cases the inverted regions extend over a very short p interval, this is e.g. the case for the initial states 6 and 7 in the $N = 5$ lattice and the initial states 7, 8 and 9 in the $N = 6$ case, whose associated $\langle n \rangle_i$'s display a single maximum very close to $p = 0$. The other reaction times displaying anomalous behavior are plotted in Fig. 6. It is noteworthy that those initial conditions for which a double inverted region is observed correspond to contiguous walker positions, whereby the heavy walker is placed at an interior site closer to the boundary or at most at the same distance from the boundary as the light walker. In contrast, those configurations with contiguous particles in which the light walker

is closer to the boundary are associated with monotonically increasing $\langle n \rangle_i(p)$ profiles, as one might intuitively expect (for large p the heavy walker can move away from the light walker more easily leaving a larger space between the boundary and itself available for the motion of the light walker). Finally, all the other initial conditions giving rise to anomalous behavior correspond to $\langle n \rangle_i(p)$ profiles displaying a single maximum as a function of p .

Let us now compare the above behavior of the local reaction time with our findings for the $N = 4$ periodic case. To begin with, note that if one switches from confining to periodic boundaries, States 2 and 5 become equivalent to, say, State 2 in the periodic case. Fig. 7 (left) displays a comparative plot for the $\langle n \rangle_i(p)$ curves in these cases. It is seen that for all values of p the reaction times $\langle n \rangle_2$ and $\langle n \rangle_5$ are well below the corresponding values of $\langle n \rangle_2$ for a periodic lattice. On the other hand, states 1, 3, 4 and 6 become equivalent to state 1 when switching to periodic boundary conditions. As seen in Fig. 7 (right) the reaction times $\langle n \rangle_{1,3,4}$ in the confining system are larger than the corresponding reaction time $\langle n \rangle_1$ in the confining case for most values of p . Exceptions are found for $\langle n \rangle_1$ and $\langle n \rangle_4$, which become smaller in the high- p regime. In contrast, the initial state 6 is the only one in which for any “temperature” the reaction is more efficient in the confining than in the periodic case.

In the cases $N = 5, 6$, one has a similar behavior of $\langle n \rangle_1$ and $\langle n \rangle_{N_s}$, i.e., there is a significant p interval where $\langle n \rangle_1$ becomes smaller than in the periodic case, whereas this interval extends to the full physical range $[0,1]$ if one starts from the N_s -th initial configuration, in which the light walker is placed at a boundary site next to the heavy walker.

Finally, we turn to the difference in behavior between the confining and the periodic case at the level of the global reaction time. In the confining case, the weights w_i used to compute $\langle n \rangle$ take a very simple form, i.e., $w_i = N_s^{-1} = 2/N(N-1)$. One thus has $\langle n \rangle = \frac{2}{N(N-1)} \sum_{i=1}^{N(N-1)/2} \langle n \rangle_i$. In addition, one can also define other global averages by averaging over subsets of initial conditions, e.g.

$$\langle n \rangle_{x_2^0=i} = \frac{1}{N-1} \sum_{x_1^0=1, x_1^0 \neq i}^N \langle n \rangle_{(x_1^0, i)} \quad (19)$$

is the average over a homogeneous subset of initial conditions with a fixed value of the heavy walker’s initial position. (In the periodic case these averages are clearly i -independent and equal to the all averaged reaction time $\langle n \rangle$). In the case of a $N = 4$ lattice, there are only two such symmetry-distinct averages, namely $\langle n \rangle_{x_2^0=1} \equiv \langle n \rangle^{BS}$ and $\langle n \rangle_{x_2^0=2} \equiv \langle n \rangle^{IS}$ with the heavy walker respectively placed at a boundary site (BS) and an interior site (IS) initially. For an arbitrary lattice size N , these global reaction times can be straightforwardly calculated from the local reaction times for each symmetry-distinct initial condition by a suitable weighting of the individual contributions. In the (particularly simple) case of the $N = 4$ lattice, all weights are equal, i.e.,

$$\langle n \rangle^{BS} = \frac{\langle n \rangle_1 + \langle n \rangle_2 + \langle n \rangle_3}{3}, \quad (20)$$

$$\langle n \rangle^{IS} = \frac{\langle n \rangle_4 + \langle n \rangle_5 + \langle n \rangle_6}{3} \quad (21)$$

As it turns out $\langle n \rangle^{BS}$ decreases monotonically with p , while $\langle n \rangle^{IS}$ first increases and then decreases (see Fig. 8). Notice that the inequality $\langle n \rangle^{BS} > \langle n \rangle^{IS}$ holds for all values of

p . In addition, one finds that $\langle n \rangle^{BS}, \langle n \rangle^{IS}$ and thus also $\langle n \rangle = \frac{\langle n \rangle^{BS} + \langle n \rangle^{IS}}{2}$ are larger than the global reaction time $\langle n \rangle$ for the periodic case, thereby emphasizing that at this level of description the confining system is less efficient over the whole temperature range. In the cases $N = 5, 6$ a similar behavior of the global reaction times is found, i.e., for a given p the global reaction times decrease when the heavy walker is shifted to the interior of the lattice, but in all cases they remain larger than in the periodic case.

As for the p -dependence of the global reaction times in the $N = 5, 6$ cases, the reaction time $\langle n \rangle^{BS} \equiv \frac{1}{N-1} \sum_{i=1}^{N-1} \langle n \rangle_i$ is found to decrease monotonically with p , whereas the other global reaction times (corresponding to configurations where the heavy walker starts from an interior site) first increase with p , thereupon reach a maximum for p well below 0.5 and finally decrease for larger p values. These maxima are again lost in the ‘‘all averaged’’ reaction time $\langle n \rangle$, which decreases monotonically with p for all lattices in the confining case, in contrast with the even-odd effect reported for periodic lattices.

4. 2D LATTICE

4.1. Periodic boundary conditions

As in the 1D case, one can take advantage of symmetry to simplify the formulation of the problem, here by lumping the $N(N-1)$ possible non-absorbing initial states (x_1^0, x_2^0) in a square planar lattice into a set of N_s states. Each symmetry-distinct initial state is now characterized by the horizontal distance d_x^0 and the vertical distance d_y^0 between the walkers (measured in lattice spacings) along the two orthogonal directions x and y specified by the vector basis of the elementary lattice cell. Both d_x^0 and d_y^0 may take values from 0 to $[\sqrt{N}/2]$, but the absorbing state with both walkers at the same site ($d_x^0 = d_y^0 = 0$) is excluded. Taking advantage of exchange symmetry with respect to d_x^0 and d_y^0 , one can therefore also exclude configurations for which, say, $d_y^0 > d_x^0$. Thus, the total number of symmetry-distinct states is ⁴ $N_s = CR_{[\sqrt{N}/2]+1}^2 - 1 = \binom{[\sqrt{N}/2]+2}{2} - 1$. To remain consistent with the numbering criterion used in the 1D case, we shall number these states from 1 to N_s by increasing Euclidean distance $d^0 = \sqrt{(d_x^0)^2 + (d_y^0)^2}$. For example, for a 3×3 lattice one has 2 symmetry-distinct states, namely:

State 1	State 2
2 - 1 - 0	2 - 0 - 0
0 - 0 - 0	0 - 1 - 0
0 - 0 - 0	0 - 0 - 0

In order to compute the reaction time and its variance, one now proceeds as in the 1D case, i.e., one first computes the corresponding $N_s \times N_s$ fundamental matrix and then respectively

⁴ In the following equation CR_A^B stands for the number of combinations with repetition of A elements choose B .

applies the equations (6) and (7) for the local quantities $\langle n \rangle_i$ and $\langle v \rangle_i$ and eqs. (2) and (9) for the global averages $\langle n \rangle$ and $\langle v \rangle$, whereby the weights w_i are again straightforward to compute.

Let us first discuss the behavior of the individual contributions $\langle n \rangle_i$ to the global reaction time $\langle n \rangle$. In the case of a 2×2 lattice, there are only two possible symmetry-distinct initial states, i.e., State 1 is a configuration in which the walkers are placed at nearest neighbor sites, whereas in State 2 is they are placed diagonal to each other. Fig. 9 (left) displays the behavior of the reaction times $\langle n \rangle_1$ and $\langle n \rangle_2$ as a function of p . While $\langle n \rangle_1$ decreases with increasing p , $\langle n \rangle_2$ increases with p at a slow rate for low values of p and more rapidly for larger values. In the case of a 3×3 lattice, the behavior of the reaction time is also different for each of the two symmetry-distinct initial conditions 1 and 2, i.e., $\langle n \rangle_1$ displays a shallow minimum as a function of p , while $\langle n \rangle_2$ is a monotonically decreasing function (see Fig. 9, right).

A careful examination of the behavior for somewhat larger periodic square planar lattices ($16 \leq N \leq 36$) suggests the following rule of thumb: those initial states for which the effective distance $\hat{d}^0 \equiv d_x^0 + d_y^0$ is even correspond to monotonically decreasing $\langle n \rangle_i(p)$ profiles, while the profiles $\langle n \rangle_i(p)$ associated with odd values of \hat{d}^0 show an inverted region. Each of these inverted regions is associated with a local minimum with respect to p , except in the 2×2 lattice case, where the inverted region extends over the whole p interval. As expected, the minimum shifts to the right with increasing value of \hat{d}^0 (see Figs. 10 and 11 for the cases of a 4×4 , 5×5 and 6×6 torus). This even-odd behavior in terms of \hat{d}^0 is analogous to the even-odd behavior in terms of d^0 observed in 1D (cf. Fig. 2).

Departures from the above rule become more frequent with increasing lattice size. An example is given by the initial state 5 corresponding to the 5×5 square planar lattice, which displays a tiny region with $\frac{d\langle n \rangle_5}{dp} > 0$ and a very shallow minimum near $p = 1$, as a careful inspection of the thick solid line in the right graph of Fig. 10 would reveal. Shortly we shall see that as a result of this inverted regions at the level of $\langle n \rangle$ also arise for sufficiently large odd values of N , in contrast with the 1D case.

Next, let us analyze the p -behavior of $\langle n \rangle$ given in Table 5. To this end, we first focusing on the case of the smallest possible lattice (2×2 lattice, corresponding to $N = 4$). Fig. 12 displays the behavior of the global reaction time $\langle n \rangle$ as a function of p for a 2×2 periodic square lattice. The inset shows that there is a small region of p -values where $\frac{d\langle n \rangle}{dp} < 0$. However, if one compares this plot to the $N = 4$ plot depicted in Fig. 4 (left), it is seen that the inverted region with $\frac{d\langle n \rangle}{dp} > 0$ is much broader in the case of a 2×2 lattice than in the case of a $N = 4$ ring, leading to a smaller value of $p_{min}^{(n)}$ in the $2D$ case. This behavior persists if one considers larger lattices with an even number of sites (compare e.g. the values of $p_{min}^{(n)}$ for $N = 16$ and $N = 36$ in Tables 2 and 6). We thus conclude that for fixed N the inverted region $[p_{min}^{(n)}, 1]$ observed for even lattices in 1D is considerably extended in 2D. Moreover, in contrast to the 1D case an inverted region also appears in the 5×5 lattice case (see the corresponding plot in Fig. 13), and numerical evidence suggests that inverted regions also arise in the 7×7 and the 9×9 cases [23].

There is another respect in which the anomalous p -behavior of $\langle n \rangle$ is here enhanced with respect to the 1D case. Let us consider the relative enhancement of the efficiency Δ in the case of an even lattice, defined as follows:

$$\Delta \equiv \frac{1}{\langle n \rangle(p = p_{min}^{(n)})} \int_{p_{min}^{(n)}}^1 \frac{d\langle n \rangle}{dp} dp = \frac{\langle n \rangle(p = 1) - \langle n \rangle(p = p_{min}^{(n)})}{\langle n \rangle(p = p_{min}^{(n)})} \quad (22)$$

From Table 7 it is seen that this quantity is very large with respect to the 1D case, even for large lattices ($N \geq 16$). On the other hand, the interval $[p_{min}^{(n)}, 1]$ corresponding to the inverted region contracts dramatically with increasing lattice size, as seen from Table 6 and expected from the arguments for the 2D case. Thus, a minute amount of asynchronicity $\delta p < 0$ brings about a drastic decrease in $\langle n \rangle$ with respect to the fully synchronous case $p = 1$.

We have also studied the global variance $\langle v \rangle$ in 2D and find a similar enhancement of the inverted regions with respect to the 1D case. The corresponding expressions for $\langle v \rangle$ and $p_{min}^{(v)}$ are listed in Tables 8 and 9. The values of $p_{min}^{(v)}$ are very close to those for $p_{min}^{(n)}$, with the exception of the 2×2 lattice, for which one respectively has $p_{min}^{(v)} \approx 0.1847$ and $p_{min}^{(n)} \approx 0.1042$.

4.2. Confining boundary conditions

In order to complete the picture of the confining case, we have investigated the reaction efficiency for two cases, namely the 3×3 and the 5×5 lattice.

Let us first discuss the 3×3 lattice. There are 12 symmetry-distinct states altogether, i.e., 5 states with the heavy walker at a corner site CS:

State 1	State 2	State 3	State 4	State 5
2 - 1 - 0	2 - 0 - 0	2 - 0 - 1	2 - 0 - 0	2 - 0 - 0
0 - 0 - 0	0 - 1 - 0	0 - 0 - 0	0 - 0 - 1	0 - 0 - 0
0 - 0 - 0	0 - 0 - 0	0 - 0 - 0	0 - 0 - 0	0 - 0 - 1

According to the numbering used in Fig. 1 (right), the above states would correspond to those for which $x_2 = 1$. There are 5 more states in which the heavy walker is positioned on a midpoint boundary site MBS. These states with $x_2 = 2$ can be pictorially represented as follows:

State 6	State 7	State 8	State 9	State 10
1 - 2 - 0	0 - 2 - 0	0 - 2 - 0	0 - 2 - 0	0 - 2 - 0
0 - 0 - 0	1 - 0 - 0	0 - 1 - 0	0 - 0 - 0	0 - 0 - 0
0 - 0 - 0	0 - 0 - 0	0 - 0 - 0	1 - 0 - 0	0 - 1 - 0

Finally, there are 2 more states in which the heavy walker sits in the centrosymmetric site CES (i.e., one has $x_2 = 5$), namely

State 11	State 12
0 - 0 - 0	0 - 0 - 0
0 - 2 - 0	0 - 2 - 0
0 - 0 - 1	0 - 1 - 0

The p behavior of the local reaction times is depicted in Fig. 14. The reaction times associated with the CS initial configurations 1-5 turn out to be monotonically decreasing in p . In contrast, the MBS configurations 6-10 and the CES configurations 11-12 are associated with reaction times displaying a single maximum. In the MBS case the maximum is located at relatively small values of p , whereas in the CES case it is found at somewhat larger p values. Interestingly, there are no initial conditions which give rise to a double inverted region, in contrast with the 1D case. These results are also confirmed by numerical simulations (data not shown).

We now compare the above results with the periodic case. If one connects the boundary sites of the confining lattice in a periodic fashion, one finds that States 1, 3, 6, 8, 10 and 12 collapse into State 1, i.e., the state in which the walkers are positioned aside of each other in the periodic lattice. On the other hand, States 2, 4, 5, 7, 9 and 11 collapse into State 2, i.e., the state in which both walkers are positioned diagonal to each other in the periodic lattice. The plots corresponding to the reaction times in the periodic case are displayed in Fig. 14 and compared to the corresponding plots for the reaction times in the confining case. For all values of p , the local reaction times are smaller in the periodic case than in all confining cases⁵. This behavior clearly differs from the 1D case, where for certain initial conditions and p -intervals the efficiency is larger in the confining case.

Finally, we consider the behavior of the global averages. Consonant with what was done in 3.2, one can define via equation (19) three global averages $\langle n \rangle^{CS} = \langle n \rangle^{x_2^0=1}$, $\langle n \rangle^{MBS} = \langle n \rangle^{x_2^0=2}$ and $\langle n \rangle^{CES} = \langle n \rangle^{x_2^0=5}$ for all three symmetry-distinct positions of the heavy walker. In the present case, these averages are related to the local reaction times as follows:

$$\begin{aligned}
\langle n \rangle^{CS} &= \frac{2\langle n \rangle_1 + \langle n \rangle_2 + 2\langle n \rangle_3 + 2\langle n \rangle_4 + \langle n \rangle_5}{8}, \\
\langle n \rangle^{MBS} &= \frac{2\langle n \rangle_6 + 2\langle n \rangle_7 + \langle n \rangle_8 + 2\langle n \rangle_9 + \langle n \rangle_{10}}{8} \\
\langle n \rangle^{CES} &= \frac{\langle n \rangle_{11} + \langle n \rangle_{12}}{2}.
\end{aligned} \tag{23}$$

The reaction time averaged over all initial conditions is

$$\langle n \rangle = \frac{4\langle n \rangle^{CS} + 4\langle n \rangle^{MBS} + \langle n \rangle^{CES}}{9} \tag{24}$$

⁵ with the exception of two initial configurations for which in the $p = 0$ limit the reactions times are found to be equal to those for the corresponding periodic cases

Fig. 15 displays the p -behavior of the three global averages and $\langle n \rangle$. As in the 1D case, the efficiency of the reaction for a given p increases as the heavy walker is moved away from the centrosymmetric site. On the other hand, one can see that $\langle n \rangle^{CS}$ decreases monotonically with p , whereas $\langle n \rangle^{MBS}$ and $\langle n \rangle^{CES}$ display a maximum. These maxima are averaged out when Eq. (24) is used to compute $\langle n \rangle$, leading as in the 1D case to monotonically decreasing behavior of $\langle n \rangle$. The global averages are all strictly larger than in the 2D periodic case, with the exception of $\langle n \rangle^{CES}$ in the limit $p \rightarrow 0$ (see Fig. 15).

We have also examined the behavior of the global averages in the 5×5 case. In this case there are 6 global averages corresponding to the 6 possible symmetry-distinct initial positions of the heavy walker characterized by Euclidian distances $d_{CES}^0 = 0, 1, \sqrt{2}, 2, \sqrt{5}, \sqrt{8}$ from the centrosymmetric site. The results obtained are entirely consistent with the findings for the 3×3 lattice, i.e., the efficiency increases when the heavy walker is moved towards the interior of the lattice. For $d_{CES}^0 \leq \sqrt{2}$ the curves $\langle n \rangle_i(p)$ display a maximum in p , whereas for larger d_{CES}^0 the decay is monotonic. Once again, the reaction time scaled by $\langle n \rangle$ and computed by averaging over all initial conditions, is monotonically decreasing.

5. GENERAL CASE

In this section we shall discuss how results for the periodic lattice case are modified if one allows for the possibility that walker 1 does not jump at a given time step. To this end, let us now assume that walker 1 and walker 2 respectively jump with probabilities p_1 and p_2 at each tick of the clock. Results for this case can be easily obtained using the approach developed in 2.2. Note that the initial scenario is recovered as a special case if one sets $p_1 \equiv 1$ and $p_2 \equiv p$.

5.1. 1D case

Let us first examine the behavior of the local reaction times $\langle n \rangle_i(p_1, p_2)$ as a function of p_2 when the value of p_1 is decreased below one. As our previous results for the $p_1 = 1$ case show, there is a monotonic decrease in the reaction time with respect to p_2 when the state number i takes even values (cf. Fig. 2) and minima in p_2 for odd values of i . Now, if one now gradually decreases p_1 , the qualitative behavior of the $\langle n \rangle_i(p_2)$ profiles does not change for even values of i , i.e. one still has $\frac{\partial \langle n \rangle_i}{\partial p_2} < 0$ for all values of p_2 . In contrast, there is a qualitative change in behavior for even values of i ; the inverted regions with $\frac{\partial \langle n \rangle_i}{\partial p_2} > 0$ vanish and one finds monotonically-decreasing profiles in this case (see Fig. 16, left). The even-odd effect in i is thus lost.

Let us now examine the p_2 behavior of the global reaction time $\langle n \rangle$ when p_1 is decreased. Analytic expressions for $\langle n \rangle$ as a function of p_1 and p_2 for periodic lattices of increasing size are given in Appendix A (see Table 10). These expressions are symmetric with respect to exchange of p_1 and p_2 . Here, for odd values of N $\langle n \rangle$ decreases monotonically with p_2 regardless of the value of p_1 , i.e., $\frac{\partial \langle n \rangle}{\partial p_2} < 0$ for all values of p_2 . In contrast, the behavior in the case of an even lattice again depends on the value of p_1 . As we have seen, for $p_1 = 1$ one has an inverted region where $\frac{\partial \langle n \rangle}{\partial p_2} > 0$. However, if one gradually decreases p_1 the minimum of $\langle n \rangle(p_2)$ is shifted to the right and below a characteristic N -dependent threshold value $p_{1,c}^{(n)}$ the inverted region finally vanishes and the curves $\langle n \rangle(p_2)$ become monotonically decreasing.

The critical values $p_{1,c}^{(n)}$ are displayed in Table 11 for periodic lattices of increasing size. These values are obtained as follows. Denote by $p_{2,min}^{(n)}$ the value of p_2 for which a minimum of $\langle n \rangle$ as a function of p_2 is observed. The value of $p_{2,min}^{(n)}$ as a function of p_1 is then easily obtained from the condition $\frac{\partial \langle n \rangle}{\partial p_2} = 0$ for $p_2 = p_{2,min}^{(n)}$. One has $\frac{\partial p_{2,min}^{(n)}}{\partial p_1} < 0$, i.e., the probability $p_{2,min}^{(n)}$ is shifted to larger values with decreasing p_1 until it becomes equal to one. This condition yields a polynomial equation in p_1 with a single root in the interval $[0,1]$; this root corresponds to the threshold value $p_{1,c}^{(n)}$ below which the profiles $\langle n \rangle_i(p_2)$ decrease monotonically. Note that one has $p_{1,c}^{(n)} \rightarrow 1$ as $N \rightarrow \infty$.

Fig. 16 (right) shows the suppression of the inverted zone in the case of the $N = 4$ lattice. Several plots of $\langle n \rangle(p_2)$ corresponding to decreasing values of p_1 are displayed. It is seen that the minimum of the curves shifts to the right with decreasing p_1 until it eventually vanishes for $p_1 < p_{1,c}^{(n)} \approx 0.834$ (cf. Table 11). Interestingly, the reaction time decreases with p_1 for a fixed value of p_2 in the region where $p_2 \lesssim 1$, while the opposite is true for not too large values of p_2 . This behavior is also confirmed by numerical simulations (data not shown).

A similar suppression of the inverted region with decreasing p_1 is also observed at the level of the global variance $\langle v \rangle$. The corresponding polynomial expressions as well as the critical values $p_{1,c}^{(v)}$ are listed in Tables 12, 13 and 14. As it turns out, the value of $p_{1,c}^{(v)}$ is almost identical to $p_{1,c}^{(n)}$ (see Tables 11 and 14).

5.2. 2D case

As in the 1D case, inverted p_2 regions are suppressed with decreasing p_1 , both at the level of the local and the global reaction times. Fig. 17 displays the behavior of the $\langle n \rangle_1$ and $\langle n \rangle$ as a function of p_2 for the 2×2 lattice. In both cases, the curves become monotonically decreasing below a given threshold value of p_1 . In contrast, the curves $\langle n \rangle_2(p_2)$ remain monotonically decreasing for any values of p_1 . The p -behavior of $\langle n \rangle$ is thus qualitatively similar to the 1D case (cf Figs. 16 and 17). The analytic expressions for $\langle n \rangle$ in terms of p_1 and p_2 as well as values of $p_{1,c}^{(n)}$ for even square lattices of increasing size are listed in Appendix B (Tables 15 and Table 16).

For 2D lattices the limiting behavior $p_{1,c}^{(n)} \rightarrow 1$ as $N \rightarrow \infty$ is the same as for 1D. Here, however, for a given number N of lattice sites the values of $p_{1,c}^{(n)}$ displayed in Table 16 are systematically smaller than those shown in Table 11. This fact suggests that in higher dimensions the inversion effect is more robust vis a vis a decrease in the mobility of walker 1. Finally, suppression of the inverted region with decreasing p_1 is also seen in the behavior of the global variance $\langle v \rangle$. The polynomial expressions for $\langle v \rangle$ and the associated values of $p_{1,c}^{(v)}$ are displayed in Tables 17 and 18.

6. DISCUSSION

Let us now summarize the main results obtained so far and introduce some physical arguments to explain them.

6.1. Results for periodic lattices

The existence of an inverted region in the case of a 1D periodic lattice is governed by a parity effect. For even values of the interparticle distance d^0 no inverted regions are observed. However, for odd values of d^0 the reaction time as a function of p displays a single minimum for a p -value larger than $1/2$, which rapidly shifts towards one with increasing d^0 and increasing lattice size. In 2D, a similar even-odd effect holds only for sufficiently small lattices; for larger lattices exceptions to this rule become increasingly frequent. On the other hand, the inverted regions become broader with respect to the 1D case and the enhancement of the reaction's efficiency within the inverted region also becomes much larger (cf. Table 7).

As already anticipated in 3.1, the above even-odd effect in 1D is closely related to the fact that in prereactive configurations where both walkers are located at contiguous sites an asynchronous step leads to reaction with a probability twice as large as for a synchronous step ($1/2$ vs. $1/4$). For such a configuration asynchronous dynamics due to a lower system temperature minimizes the probability of mutual avoidance once the particles are within the interaction zone (in which the next time step may lead to reaction). For sufficiently high values of p the number of statistical paths leading to such nearest-neighbor configurations are higher for odd values of d^0 than for even values. In this high p regime, the reaction time increases with p for odd d^0 , while it decreases with p for even values of d^0 . The number of initial conditions with odd values of d^0 is larger for an even value than for an odd value of N ; thus the total increase in p of the associated reaction times in the former case overcomes the p -decrease of the reaction times associated with even-valued initial distances and the global reaction time $\langle n \rangle$ increases.

In 1D, the size of the inverted region for odd values of the interparticle distance d^0 must decrease with increasing d^0 (Fig. 2) or increasing lattice size N (Fig. 3), since discrete diffusion over long distances becomes the rate limiting step. In 2D, the enhancement of the even-odd effect with respect to the 1D case can be understood as follows. For a given number of sites N , the initial-condition-averaged distance between the particles is smaller than in 1D, thereby reducing the role of long-distance hopping with respect to mutual avoidance in the interaction zone. In addition, the probability of reaction for nearest-neighbor configurations in a sufficiently large lattice is four times higher for an asynchronous than for a synchronous step ($1/4$ vs. $1/16$).

Finally, we have seen that the inverted regions in the periodic case are suppressed if the mobility of the light walker lies below a size-dependent threshold value. This is reasonable, since a prerequisite for the onset of the even-odd effect is that both particles must first have a minimal mobility to come into the vicinity of each other. If this is not the case, the dynamics is controlled by the relative diffusion coefficient, which is a monotonically increasing function of p_1 and p_2 .

6.2. Results for confining lattices

In small confining lattices the behavior of the reaction time is even more complex. In 1D, the reaction time may decrease monotonically, increase monotonically, display a single maximum or even a maximum and a minimum, giving rise to inverted regions in the last three cases (cf. Fig. 5). Those initial conditions with the heavy walker at a boundary site do not give rise to inverted regions, whereas all the others do. Initial configurations where the

light walker is on a boundary site and the heavy walker is next to it result in reaction times which increase monotonically with p , thereby giving rise to an inverted region of maximum size. In particular, the $p = 0$ case (one walker plus trap case) then becomes more efficient than the $p = 1$ case (case of identical walkers). Double inverted regions are observed for those initial states where both walkers are at interior sites next to each other with the light walker closer to the lattice boundary or at the same distance from the boundary as the heavy walker. In contrast, no double inverted regions are observed in the 2D cases studied.

Both in the 1D and the 2D case, the global reaction time $\langle n \rangle_{x_2^0=i}$ (average over the positions of the light walker) displays a local maximum as a function of p as long as the heavy walker starts sufficiently close to the geometric center of the lattice, and it decays monotonically with p as the heavy walker is shifted away from the center (cf. Figs. 8 and 15). The reaction time $\langle n \rangle$ is found to decrease monotonically with increasing p , in contrast with the case of a periodic lattice with an even number of sites.

This complex behavior for confining boundary conditions can, at least in 1D, be understood in terms of a description based on the concept of a “fluctuating” lattice. To illustrate the use of such a metaphor, consider the 1D case subject to the choice $p = 0$. Here, walker 2 plays the role of an immobile trap which divides the lattice into two disconnected sublattices. Depending on its initial position, walker 1 will perform a random walk between the reflecting and the absorbing boundary of one of these sublattices. From the standpoint of the reaction time (see Fig. 18), the motion of walker 1 in each sublattice is equivalent to its motion in a periodic lattice. For most initial conditions, the size of the corresponding periodic lattice is larger than the size of the original confining lattice, implying that for a given value of N the reaction time (a monotonically increasing function of N) also becomes larger than in the periodic case. Thus, in the small p limit the reaction is less efficient in the confining case than in the periodic case. An exception is found for the $N(N - 1)/2$ -th initial condition (see e.g. the curve for $\langle n \rangle_6$ in Fig. 7, right), for which the effective size of the associated periodic lattice is smaller than N . Such configurations are no longer found in the 2D cases we have examined, where periodic lattices are more efficient than confining ones, with the exception of two cases in the limit $p \rightarrow 0$ for which the efficiency becomes the same (cf. Fig. 14). This behavior is due to the fact that the trapping effect exerted by the heavy walker and the confining lattice boundary on the light walker is lost in higher dimensions.

If one now slowly increases p , the above effective description in terms of a periodic lattice remains valid, since walker 2 remains a deep trap. However, the fact that walker 2 can now move leads to time fluctuations of the lattice size of the associated periodic lattice. In the case where walker 2 starts off from a boundary site (corresponding to the first N initial conditions), fluctuations can only lead to a smaller effective size than the initial one, resulting in a monotonic decrease of the reaction time with respect to the $p = 0$ case. However, for any other initial condition with walker 2 at an interior site small fluctuations in the position of the trap can in many cases lead to a larger effective size, resulting in an increase of the reaction time. On the other hand, for somewhat larger values of p excursions of walker 2 towards the boundaries become more frequent, resulting in a more efficient confinement of walker 1 and thereby in a decrease of the reaction time. In other words, the effect due to lattice size fluctuations is overcome by the significant increase in the relative diffusion coefficient, which is a monotonically increasing function of p [21]. The reaction time, which in a continuum description is inversely proportional to the diffusion coefficient, will therefore decrease with p in this regime. As a result of the combination of the above low- p and high- p

effects, for those configurations where walker 2 is sufficiently far from the boundary and the initial particle separation is sufficiently large (such that the continuum picture applies for sufficiently large p) the reaction time first increases and then decreases with p .

The additional increase of the reaction time with p in the high p region for the subset of initial conditions associated with a double inverted region can possibly be explained in terms of an enhancement of mutual avoidance effects when particles are close to each other and far from the boundary ⁶, resulting in an increased escape probability. The absence of this additional high- p inverted region in the 2D case is probably due to the existence of additional degrees of freedom which no longer make a description in terms of the periodic case possible. One could therefore expect that the even-odd effect leading to the high- p inverted region does no longer hold and that the dynamics is essentially governed by long-range diffusion, resulting in a p -decrease of the reaction time.

In 1D, the disappearance of the inverted region associated with the the global encounter time $\langle n \rangle_{x_2^0=i}$ as walker 2 is shifted away from the inmost lattice sites to the boundaries could be explained by the fact that lattice size fluctuations responsible for the low p inverted region play a less important role when the initial distance between the walkers becomes larger. Clearly, the average of the interparticle distance over the positions of walker 1 becomes larger when walker 2 is shifted away from the centrosymmetric site.

Finally, the monotonic decrease of the global reaction time $\langle n \rangle$ over the whole p range can be explained as follows. In the small p limit the effective shortening of the lattice through the motion of walker 2 from the boundary to the bulk for the first N initial conditions overcomes the effective increase in system size for the other initial conditions. In the opposite limit of large p , the even-odd effect leading to mutual avoidance in the effective periodic-lattice description is weakened due to the lattice size fluctuations, and the global reaction time decreases.

7. CONCLUSIONS

The principal conclusion that can be drawn from the study presented in this paper is that, in characterizing the efficiency of (two-channel) reactions between independently-mobile reactants on a lattice, for small systems one may find regimes where, counter one's intuition, the reaction efficiency can decrease with increasing "temperature." Moreover, both minima and maxima in the reaction efficiency have been found and quantified, thus establishing the existence of one or more "inverted regions." We stress that, in contrast to Marcus theory, the emergence of these anomalous regions is a consequence of a (strictly) classical interplay between system geometry and individual particle dynamics (and the importance of interactions within a certain reaction radius or "zone"). We have demonstrated and quantified that these inverted regions arise in 1D and 2D lattices for a wide class of initial conditions. Also, we note that numerical evidence has been presented in [23] that the effect is present in 3D, and for cases where the reaction "rules" are different from the ones adopted in this work [33].

So that the plethora of results reported here not obscure a principal insight, we emphasize that the discrete character of the geometric support is an important (perhaps critical) ingredient in generating the emergence of an inverted region. It is precisely the discrete geometry

⁶ Recall that double inverted regions are associated with initial conditions which fulfil these two conditions.

of the lattice which allows one to distinguish between reaction channels (viz., irreversible termination of the reaction owing to same site occupancy or nearest-neighbor crossing). Such distinctions are lost in the continuum limit, where the efficiency of a diffusion-reaction process is characterized universally by an increase in reaction efficiency with respect to an increase in system temperature.

In the cases we have studied here, much of the observed anomalous behavior can be understood in terms of a competition between diffusional transport over long distances and the probability of mutual avoidance inside the interaction zone. A very large jump probability p may favor transport over long distances, since it increases the relative diffusion coefficient. However, it may also decrease the residence time in the interaction zone. As we have seen, the latter effect may become dominant in sufficiently small lattices and thus determine the anomalous decrease of the efficiency with temperature. Remarkably, the fluctuation-driven resonance and antiresonance phenomena reported in this work do not involve coloured noise, in contrast with other first-passage problems such as resonant activation [35].

The study presented here was motivated to a large extent by the remarkable and unexpected results found in studying experimentally systems at the nanolength scale. It is premature to suggest that the effects uncovered here might be found in a particular experiment, but it is certainly not premature to note that the sophistication of these experiments has now reached a point where the presence of an "inversion regime" might be explored.

From a theoretical point of view, there are many facets of the present problem that need to be developed. For example, one can study the effect of modifying the reaction rules. In this context, the case of a reaction probability $p_R < 1$ per collision is particularly interesting. An enhancement of the anomalous behavior can be expected in this case, since the efficiency of recollisions in the interaction zone can be strongly diminished by amplifying the simultaneous motion of the two reactants. Such counterintuitive effects are rather common in binary reaction systems. For example, Saxton has recently considered a binary reaction with $p_R < 1$ between two simultaneously moving walkers in a percolation cluster with blocking sites [36]. This model was recently proposed to explain protein motion in lipid rafts. Saxton came to the interesting conclusion that at sufficiently low reaction rates increasing the obstacle concentration might result in an anomalous decrease of the reaction time due to an enhancement of recollisions in the interaction zone. Similar effects are currently being investigated for binary reactions in other types of disordered media, e.g. so-called small-world networks, in which a very small number of long-range connections between sites may have drastic effects upon the reaction time.

Finally, since non-nearest neighbor jumps [22] are likely to become of increasing importance with an increase in the system temperature, it is of some interest to incorporate this facet into the present model. Moving from a scenario in which one analyzes the problem in terms of a symmetric random walk, incorporating "drift" and accounting for deactivation by regular or periodic impurities in the system opens up connections to an even broader range of experimental phenomena. It may be hoped that the new insights arising from the study of the above systems along with non-classical approaches will help to improve the current understanding of encounter-controlled processes in small-size systems.

8. ACKNOWLEDGMENTS

We thank J. L. Bentz for a comprehensive numerical check of our results for the 3×3 confining lattice and the general 1D case treated in 5.1 and Prof. G. Nicolis for helpful

discussions.

-
- [1] A. Karlsson, R. Karlsson, M. Karlsson, A.S. Cans, A. Stromberg, F. Ryttsen and O. Orwar, *Nature* **409**, 150 (2001).
 - [2] D. T. Chiu, C.F. Wilson, A. Karlsson, A. Danielsson, A. Lundqvist, A. Stromberg, F. Ryttsen, M. Davidson, S. Nordholm, O. Orwar and R. N. Zare, *Chem. Phys.* **247**, 133 (1999).
 - [3] D. T. Chiu, C. F. Wilson, F. Ryttsen, A. Stromberg, C. Farre, A. Karlsson, S. Nordholm, A. Gaggar, B. P. Modi, A. Moscho, R. A. Garza-Lopez, O. Orwar and R. N. Zare, *Science* **283**, 1892 (1999).
 - [4] A. A. Ovchinnikov and Y. B. Zeldovich, *Chem. Phys.* **28**, 215 (1978).
 - [5] D. Toussaint and F. Wilczek, *J. Chem. Phys.* **78** 2642 (1983).
 - [6] G. H. Weiss, *Aspects and applications of the random walk*, North-Holland Elsevier Science B.V, Amsterdam (1994).
 - [7] S. Redner, *A Guide to First-Passage Processes*, Cambridge University Press, Cambridge (2001).
 - [8] U. Seiferheld, H. Baessler and B. Movaghar, *Phys. Rev. Lett.* **51**, 813 (1983).
 - [9] Z. Rácz, *Phys. Rev. Lett.* **55**, 1701 (1985).
 - [10] S.A. Rice, in *Diffusion-Limited Reactions*, edited by C. H. Bamford, C. F. H. Tipper, and R. G. Compton, Elsevier, Amsterdam (1985).
 - [11] P.L. Krapivsky and S. Redner, *J. Phys. A* **29**, 5397 (1996).
 - [12] S. Redner and K. Kang, *J. Phys. A* **17**, L451 (1984).
 - [13] A. Blumen, G. Zumofen and J. Klafter, *Phys. Rev. B* **30**, 5379 (1984).
 - [14] M. Bramson and J. L. Lebowitz, *Phys. Rev. Lett.* **61**, 2397 (1988).
 - [15] A. Szabo, R. Zwanzig and N. Agmon, *Phys. Rev. Lett.* **61**, 2496 (1989).
 - [16] A. J. Bray and R. A. Blythe, *Phys. Rev. Lett.* **89**, 150601 (2002).
 - [17] G. Oshanin, O. Bénichou, M. Coppey and M. Moreau, *Phys. Rev. E* **66**, 060101 (2002).
 - [18] M. Moreau, G. Oshanin, O. Bénichou and M. Coppey, *Phys. Rev. E* **67**, 045104 (2003).
 - [19] M. Moreau, G. Oshanin, O. Bénichou and M. Coppey, *Physica A* **327**, 99 (2003).
 - [20] J. J. Kozak, C. Nicolis and G. Nicolis, *J. Chem. Phys.* **113**, 8168 (2000).
 - [21] J. L. Bentz, J. J. Kozak, E. Abad and G. Nicolis, *Physica A* **326**, 55 (2003).
 - [22] J. L. Bentz, J. J. Kozak and G. Nicolis, *Physica A* **353**, 73 (2005).
 - [23] E. Abad, G. Nicolis, J. L. Bentz and J. J. Kozak, *Physica A* **326**, 69 (2003).
 - [24] R. A. Marcus, *J. Chem. Phys.* **24**, 966 (1956).
 - [25] R. A. Marcus, *Can. J. Chem.* **37**, 155 (1959).
 - [26] R. A. Marcus, *Annu. Rev. Phys. Chem.* **15**, 155 (1964).
 - [27] G. L. Closs and J. R. Miller, *Science* **240**, 440 (1988).
 - [28] H.B. Gray and J.R. Winkler, *Q. Rev. Biophys.* **36**, 341 (2003).
 - [29] H.B. Gray and J.R. Winkler, *Proc. Natl. Acad. Sci. (USA)* **102**, 3534 (2005).
 - [30] J. E. Kemeny and J. L. Snell, *Finite Markov chains*, Van Nostrand, Princeton (1960).
 - [31] E. Abad, *AIP Conference Proceedings* **779**, 149 (2005).
 - [32] E. W. Montroll, *J. Math. Phys.* **10**, 753 (1969).
 - [33] E. Abad, *Phys. Rev. E* **72**, 021107 (2005).
 - [34] C. A. Walsh and J. J. Kozak, *Phys. Rev. B* **26**, 4166 (1982).
 - [35] See e.g. C. R. Doering and T. C. Elston in *Nonequilibrium Statistical Mechanics in One*

- Dimension*, ed. by V. Privman, Cambridge University Press (1997), pages 360-365.
- [36] M. J. Saxton, J. Chem. Phys. **116**, 203 (2002).

Tables in the main body

N	$\langle n \rangle$
2	$2/(2-p)$
3	2
4	$(10/3)(3p-4)/(p^2+2p-4)$
5	$4(2p-5)/(p^2-4)$
6	$(28/5)(p^2-10p+10)/(p^3-4p^2-4p+8)$
7	$(4/3)(p^2+8p-14)/(p^2-2)$
8	$(12/7)(13p^3+6p^2-126p+112)/((p-2)(p^3+6p^2-8))$
9	$10(2p^3-5p^2-16p+24)/((p^2+2p-4)(p^2-2p-4))$
10	$(22/9)(7p^4-76p^3+16p^2+288p-240)/(p^5-6p^4-12p^3+32p^2+16p-32)$

TABLE 1: Analytic expressions for $\langle n \rangle$ (1D periodic lattices of increasing size N)

N	$p_{min}^{(n)}$
2	.000000
4	.666667
6	.859648
8	.920393
10	.948308
12	.963611
14	.972951
16	.979086
18	.983337
20	.986407
22	.988698
24	.99045
26	.99183
28	.99292
30	.99381
32	.99455
34	.99515
36	.99567

TABLE 2: Values of $p_{min}^{(n)}$ (1D periodic lattices of increasing size N)

N	$\langle v \rangle$
2	$2p/(2-p)^2$
3	2
4	$(2/3)(192 - 316p + 152p^2 - 15p^3)/(p^2 + 2p - 4)^2$
5	$4(-2p^3 + 25p^2 - 80p + 84)/(p^2 - 4)^2$
6	$(28/5)(-1096p + 768p^2 - 206p^3 + 28p^4 - p^5 + 512)/(8 - 4p + p^3 - 4p^2)^2$
7	$(4/3)(-320p + 88p^2 + 8p^3 + p^4 + 252)/(p^2 - 2)^2$
8	$(12/7)(-13p^7 + 252p^6 + 546p^5 - 4736p^4 - 2184p^3 + 35520p^2 - 50848p + 21504)/((p^3 + 6p^2 - 8)^2(p - 2)^2)$
9	$2(-10p^7 + 253p^6 - 816p^5 - 2748p^4 + 11872p^3 + 5552p^2 - 42496p + 29568)/((p^2 - 2p - 4)^2(p^2 + 2p - 4)^2)$

TABLE 3: Analytic expressions for $\langle v \rangle$ (1D periodic lattices of increasing size N)

N	$p_{min}^{\langle v \rangle}$
2	.000000
4	.666667
6	.852189
8	.914315
10	.943742

TABLE 4: Values of $p_{min}^{\langle v \rangle}$ (1D periodic lattices of increasing size N)

N	$\langle n \rangle$
4	$(2/3)(40 - 31p)/(-p^2 - 6p + 8)$
9	$8(9 - 2p)/(8 - p^2)$
16	$(8/45)(1191p^3 + 252p^2 - 14252p + 13184)/(3p^4 + 24p^3 - 56p^2 - 96p + 128)$
25	$(76/3)(-9p^3 + 2p^4 + 320 - 124p^2 - 48p)/(p^5 + 4p^4 - 44p^3 - 144p^2 + 64p + 256)$
36	$(2/1225)(169521024p^3 - 99291648p^2 - 21958740p^5 + 760284p^6 + 247652352 - 296662016p + 494505p^7 + 614144p^4)/(5376p^3 - 8704p^2 - 1176p^5 - 256p^6 - 6144p + 8192 + 54p^7 + 5p^8 + 2688p^4)$

TABLE 5: Polynomial expressions for $\langle n \rangle$ (2D periodic square planar lattices of increasing size N)

N	$p_{min}^{(n)}$
4	.104208
16	.750207
36	.840892

TABLE 6: Values of $p_{min}^{(n)}$ (2D periodic square planar lattice of increasing (even-valued) size N)

N	$\Delta(1D)$	$\Delta(2D)$
4	0.111	0.802
16	0.067	0.416
36	0.016	0.344

TABLE 7: Relative enhancement Δ of the global reaction time for 1D periodic lattices and 2D periodic square planar lattices with the same number of sites N .

N	$\langle v \rangle$
4	$-(2/3)(1240p + 31p^3 - 560p^2 - 768)/(p^2 + 6p - 8)^2$
9	$-8(288p + 2p^3 - 49p^2 - 584)/(p^2 - 8)^2$
16	$-(8/135)(195677696p + 15943296p^4 - 5833248p^3 - 115741696p^2 - 511812p^5 - 705816p^6 + 10719p^7 - 88932352)/(3p^4 + 24p^3 - 56p^2 - 96p + 128)^2$
25	$-(4/3)(16064512p - 8024128p^4 - 3642368p^3 + 35447808p^2 - 2255p^8 - 48480256 - 813472p^5 + 187628p^6 + 10448p^7 + 38p^9)/(p^5 + 4p^4 - 44p^3 - 144p^2 + 64p + 256)^2$
36	$-(2/8575)(1690178540273664p - 9697076228p^{13} + 226056069312p^{12} + 17307675p^{15} + 1052496354082816p^4 - 1589772806520832p^3 - 494222977269760p^2 + 435557221152p^{11} + 87781881765888p^8 + 477281389805568p^5 - 477098773250048p^6 - 39787096070144p^7 - 7123662261248p^{10} - 2654087139328p^9 - 697746159828992 - 2669903720p^{14}) / (-6144p + 2688p^4 + 5376p^3 - 8704p^2 + 5p^8 + 8192 - 1176p^5 - 256p^6 + 54p^7)^2$

TABLE 8: Polynomial expressions for $\langle v \rangle$ (2D periodic square planar lattice of increasing size N)

N	$p_{min}^{(v)}$
4	.184684
16	.748812
36	.840409

TABLE 9: Values of $p_{min}^{(v)}$ (2D periodic square planar lattice of increasing (even-valued) size N)

Figures

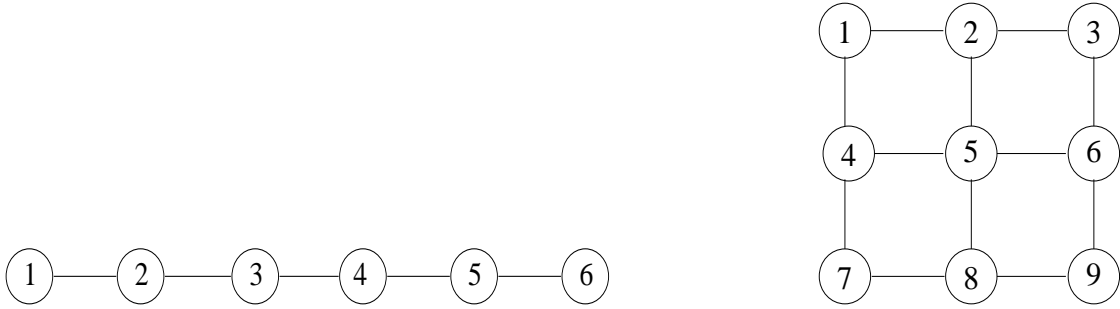


FIG. 1: Integer coordinates associated with each site for a 1D lattice with $N = 6$ (left) and a 2D lattice with $N = 9$ (right).

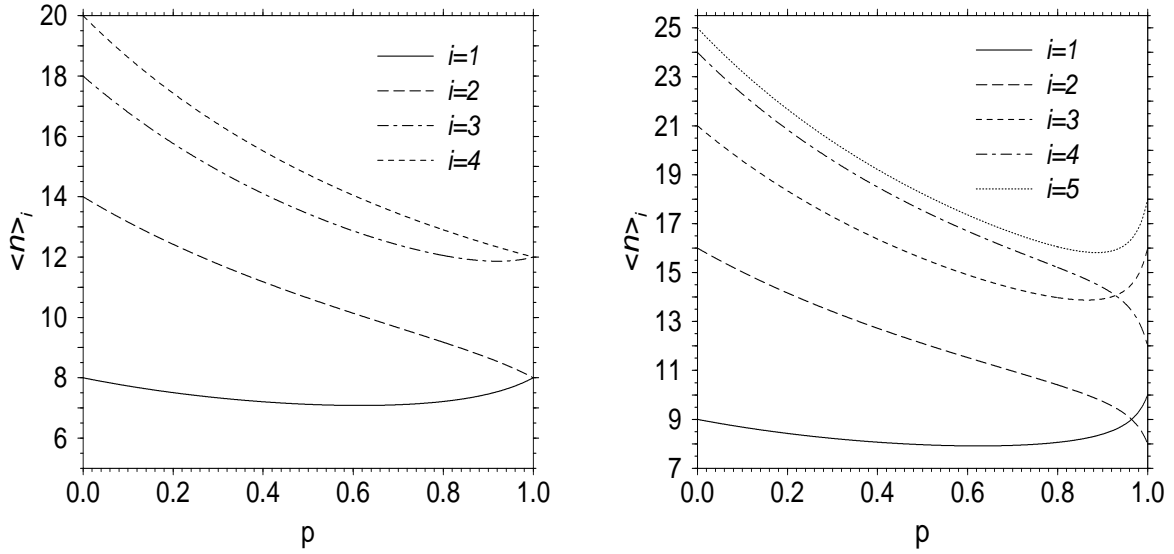


FIG. 2: p -behavior of the local reaction times in a $N = 9$ case (left) and the $N = 10$ case (right).

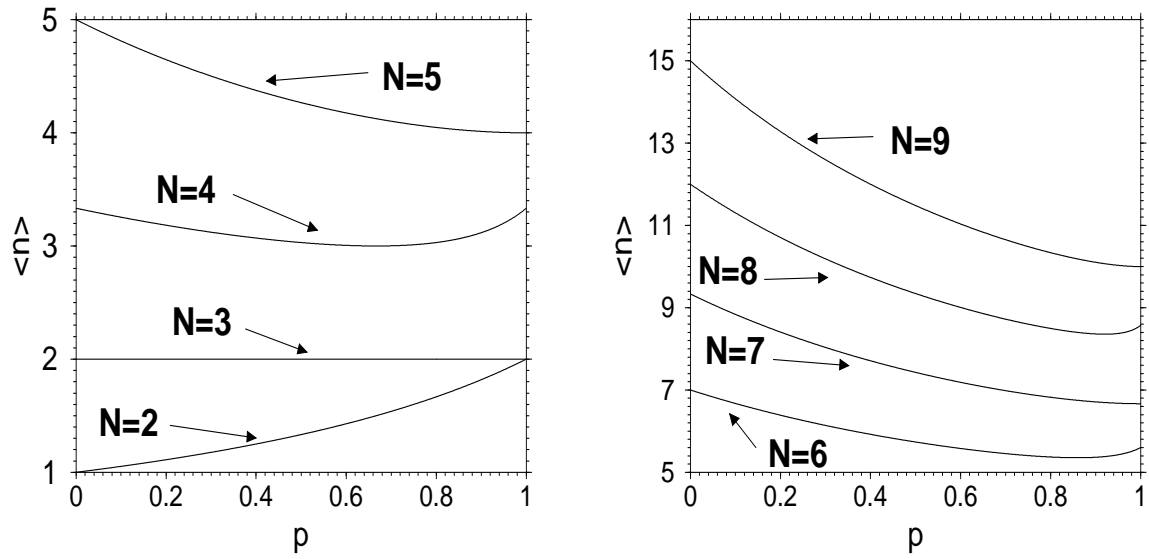


FIG. 3: Global reaction time $\langle n \rangle$ as a function of p for $N = 2, \dots, 5$ (left) and $N = 6, \dots, 9$ (right).

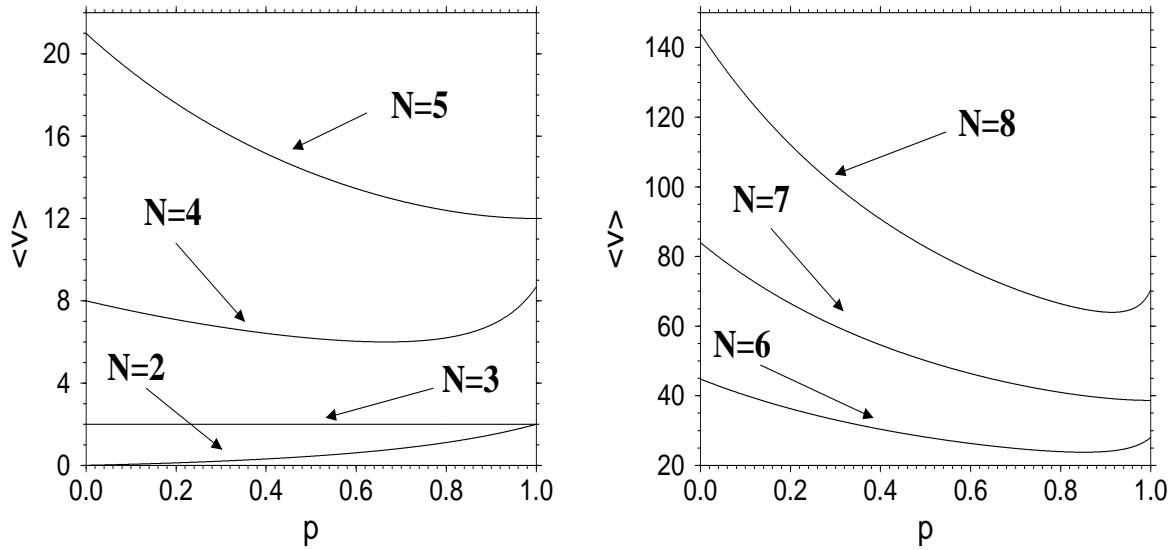


FIG. 4: Global variance $\langle v \rangle$ as a function of p for $N = 2, \dots, 5$ (left) and $N = 6, \dots, 8$ (right).

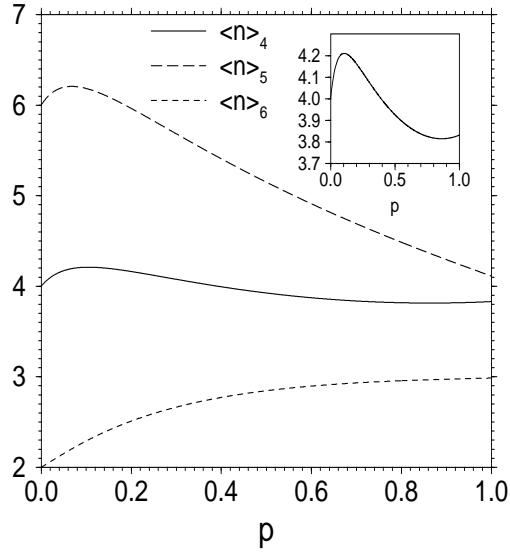


FIG. 5: p -Behavior of the local reaction times for those initial conditions characterized by the onset of an inverted region (1D lattice with $N = 4$) The inset clearly shows the double inverted region displayed by $\langle n \rangle_4$.

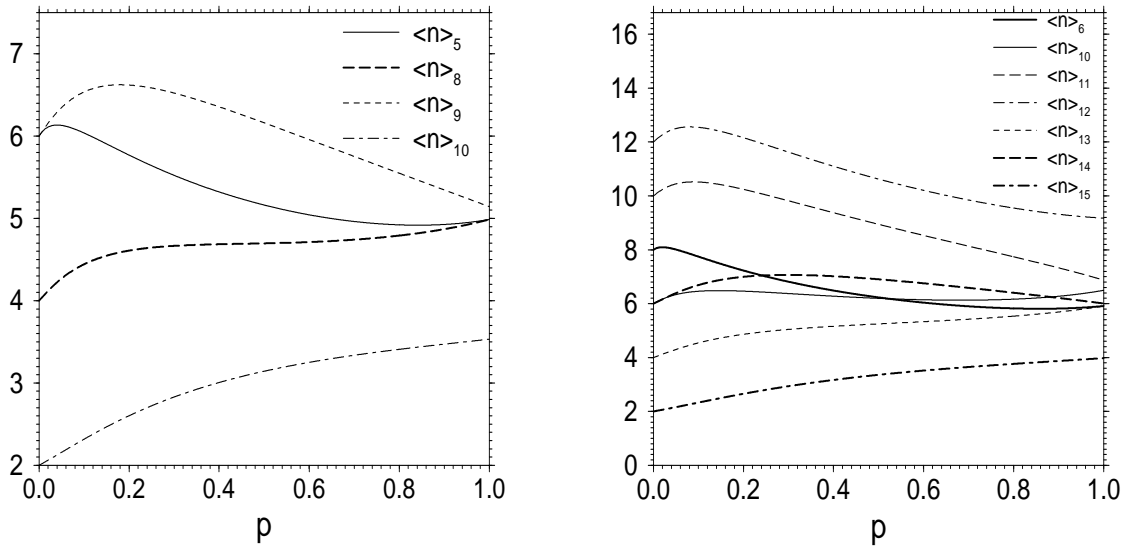


FIG. 6: p -Behavior of the local reaction times for some of the initial conditions characterized by the onset of an inverted region. The left (right) graph corresponds to a 1D lattice with $N = 5(N = 6)$.

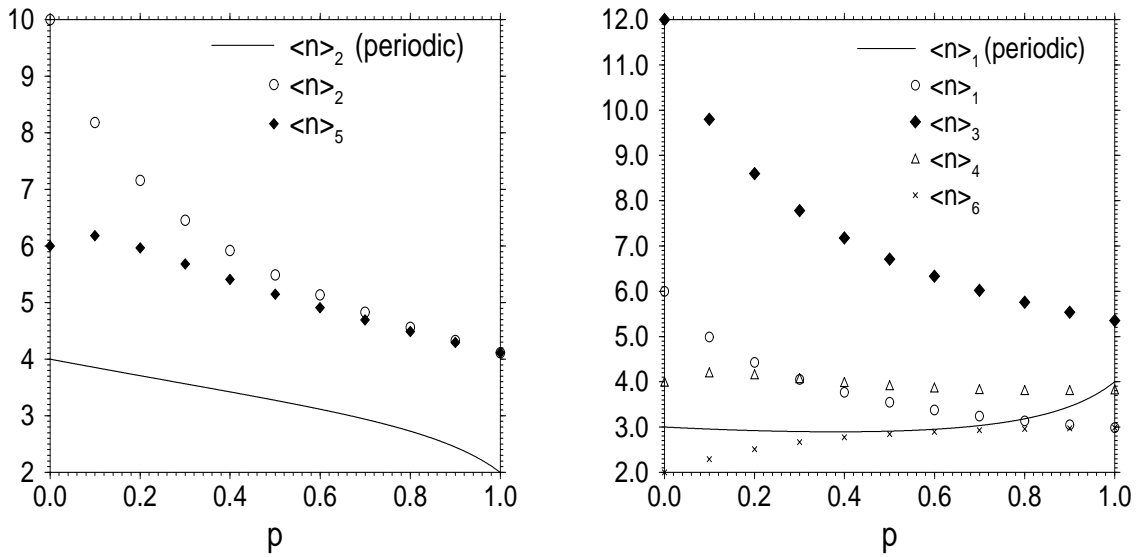


FIG. 7: p -behavior of the local reaction times in the confining and the periodic $N = 4$ case. The initial states 2 and 5 in the confining lattice collapse to the initial state 2 (corresponding to walkers at next to nearest sites in the periodic lattice) when the lattice boundary sites are connected to each other (see left graph). The initial states 1, 3, 4 and 6 in the confining lattice collapse to the initial state 1 (corresponding to contiguous walkers in a periodic lattice) when the lattice boundary sites are connected to each other (see right graph).

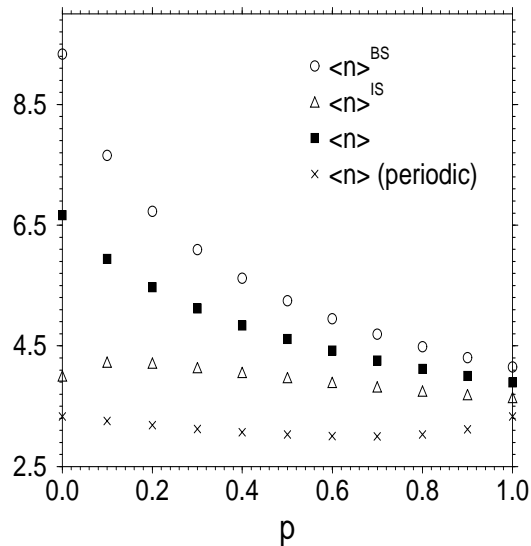


FIG. 8: p -Behavior of the global reaction times for the periodic and the confining $N = 4$ case.

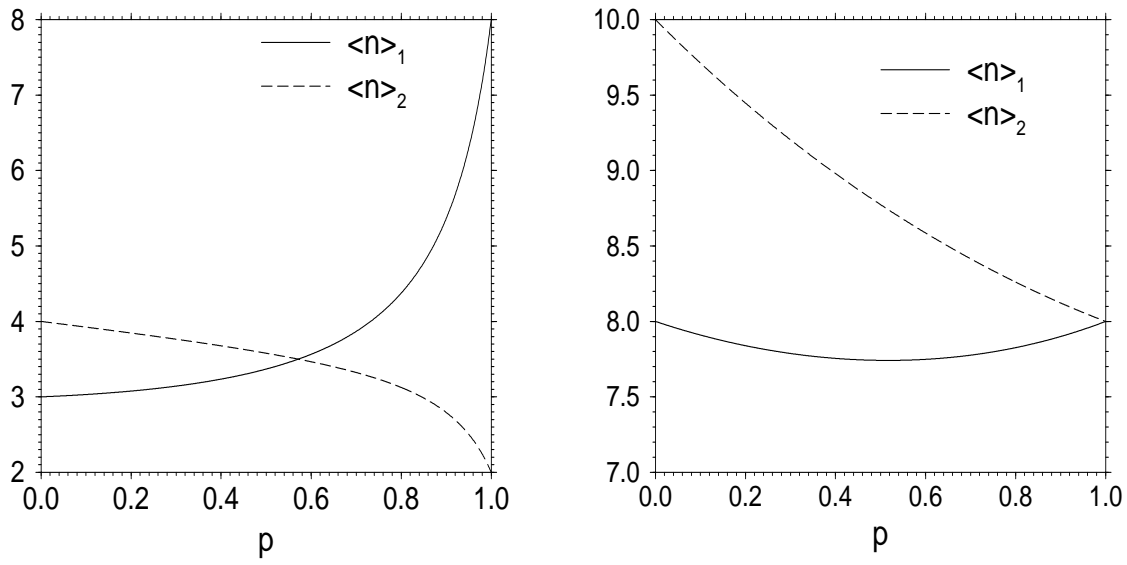


FIG. 9: p -Behavior of the local reaction times $\langle n \rangle_1$ and $\langle n \rangle_2$ in a 2×2 (left) and a 3×3 periodic square planar lattice (right). The values of the effective distance \hat{d}^0 associated with the initial state 1 and 2 are respectively 1 and 2.

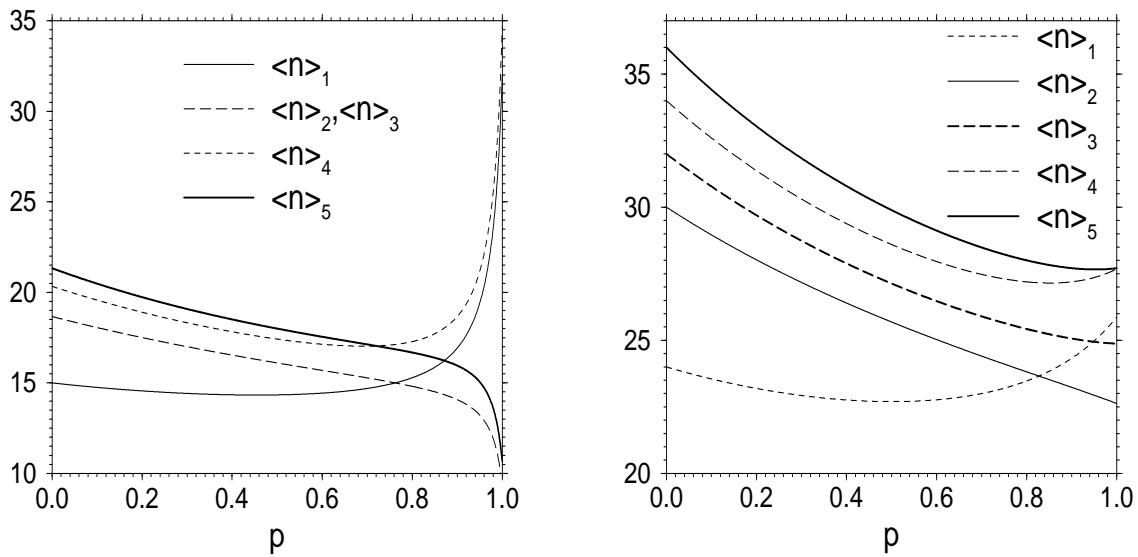


FIG. 10: p -Behavior of the local reaction times for each of the five symmetry-distinct initial configurations in a 4×4 square planar lattice (left) and a 5×5 square planar lattice (right). In both cases the values of \hat{d}^0 associated with the initial states 1, 2, 3, 4 and 5 are respectively 1, 2, 2, 3 and 4.

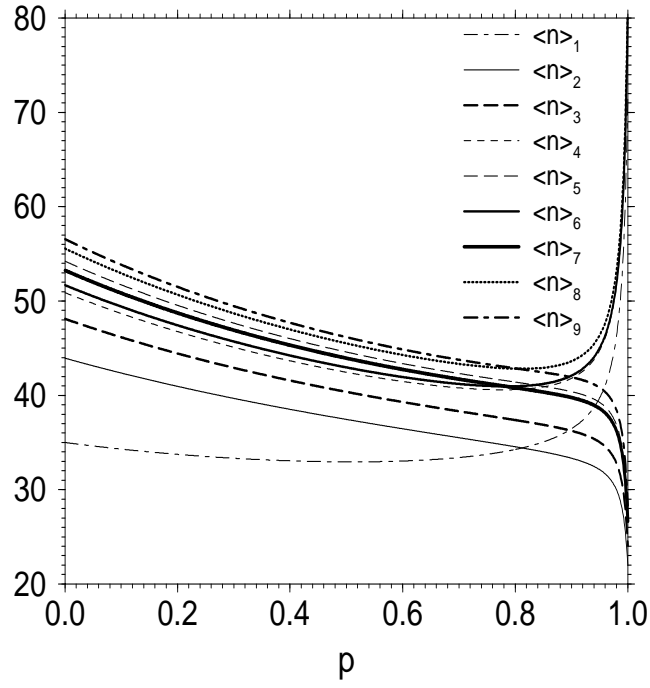


FIG. 11: p -Behavior of the local reaction times for each the 9 symmetry-distinct initial configurations in a 6×6 square planar lattice. The values of d^0 associated with the initial states 1, 2, 3, 4, 5, 6, 7, 8 and 9 are respectively 1, 2, 2, 3, 4, 3, 4, 5 and 6.

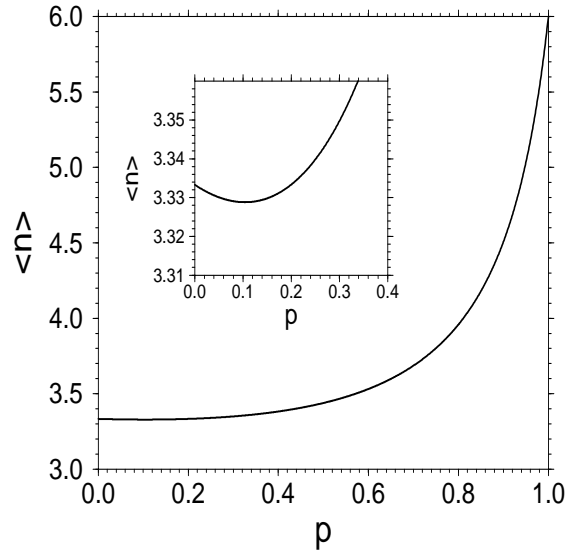


FIG. 12: p -behavior of $\langle n \rangle$ in an $N = 4$ periodic square planar lattice. The inset shows the minimum of the curve for $p \approx 0.104$.

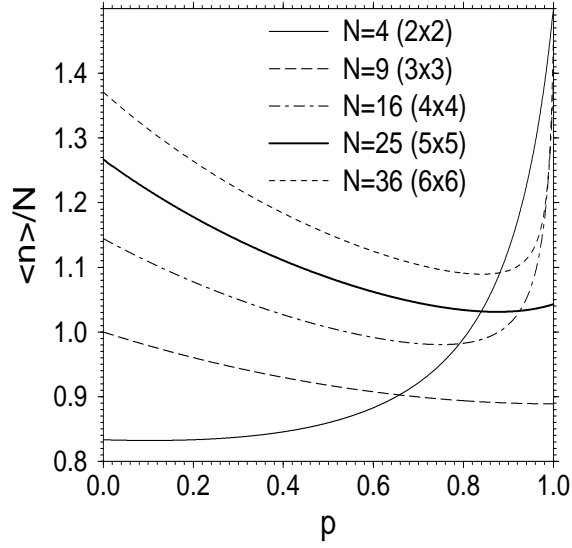


FIG. 13: p -Behavior of the global reaction time (divided by the lattice size) for 2D square planar lattices of increasing size.

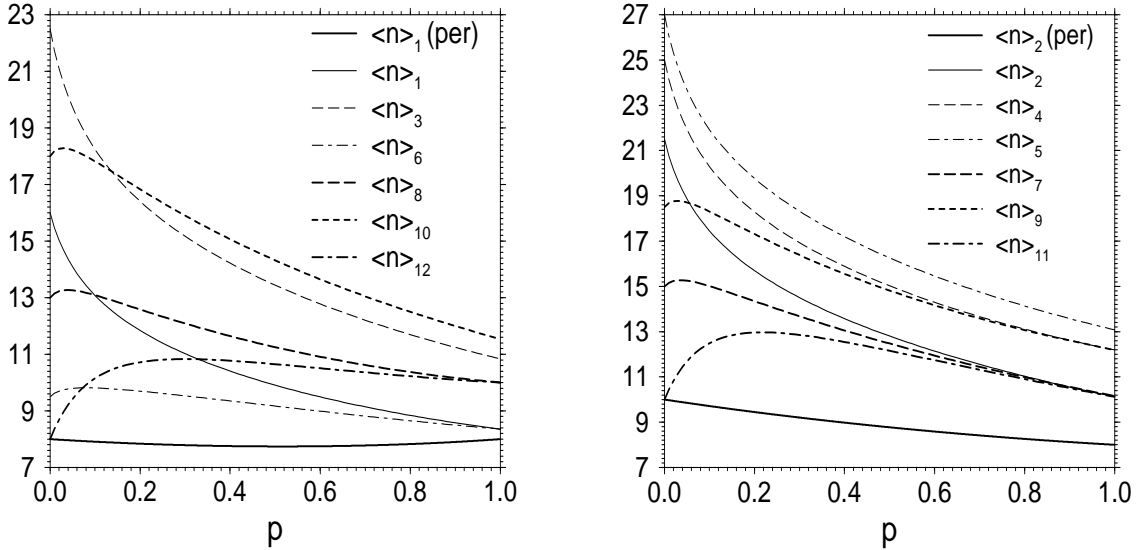


FIG. 14: p -behavior of the local reaction times in the confining 3×3 case. The initial states 1, 3, 6, 8, 10 and 12 in the confining case collapse to the same state when the boundary sites are connected periodically, i.e., State 1 with contiguous walkers in the periodic lattice (see left graph). The initial states 2, 4, 5, 7, 9 and 11 also collapse to the same state, i.e., State 2 corresponding to walkers placed diagonally in the periodic lattice (see right graph). The thick solid lines show the p -behavior in the periodic case.

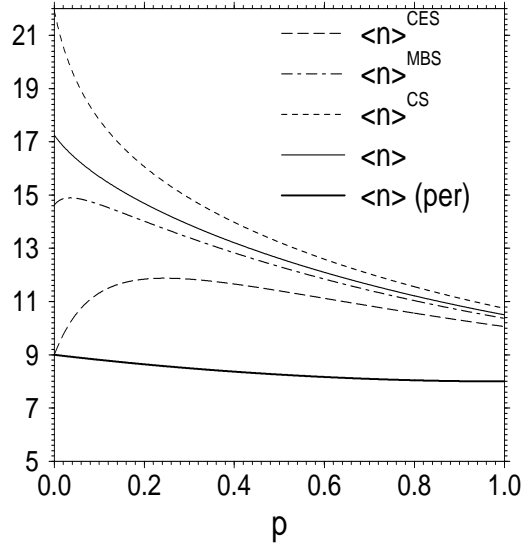


FIG. 15: p -Behavior of the global reaction times in the confining 3×3 case. The thick solid line corresponds to the behavior of $\langle n \rangle$ in the periodic 3×3 case.

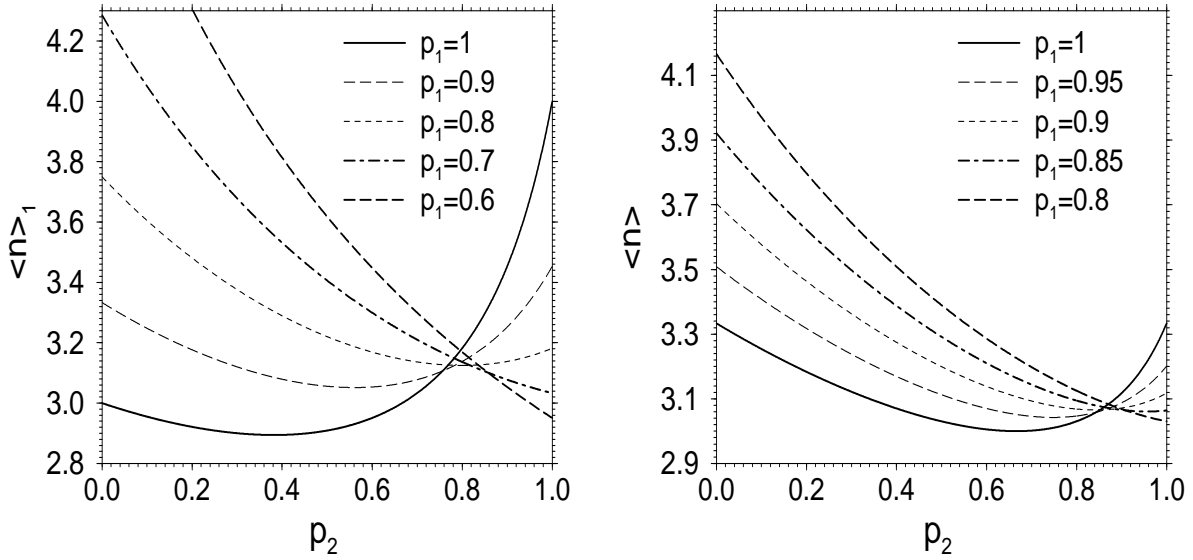


FIG. 16: Behavior of the curves $\langle n \rangle_1(p_2)$ (left) and $\langle n \rangle(p_2)$ (right) for different values of p_1 in a periodic 1D lattice with $N = 4$.

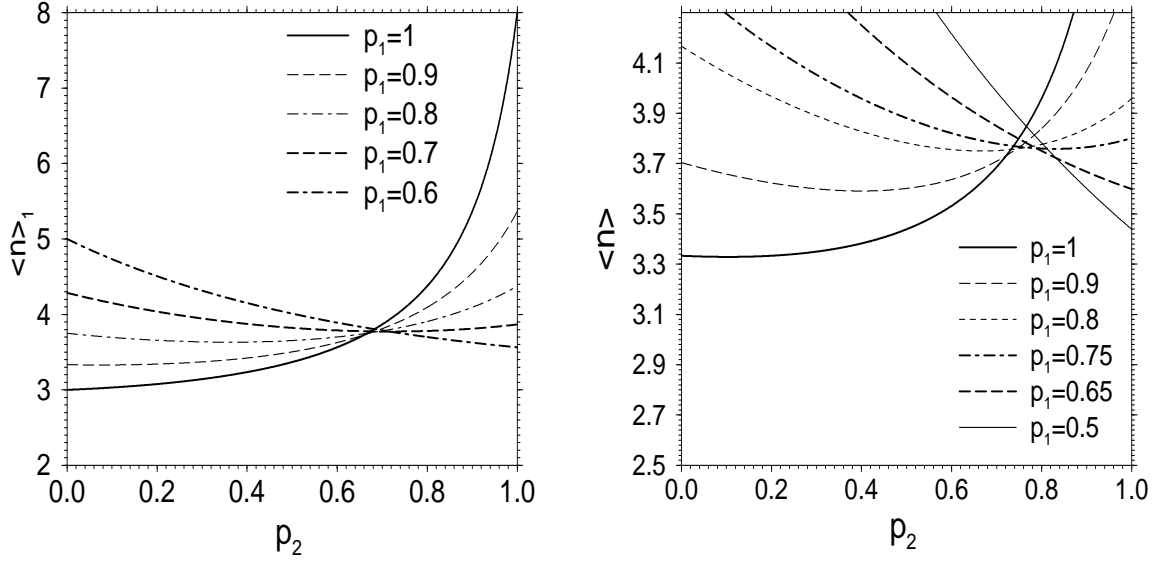


FIG. 17: Behavior of the curves $\langle n \rangle_1(p_2)$ (left) and $\langle n \rangle(p_2)$ (right) for different values of p_1 in a 2×2 periodic square planar lattice.

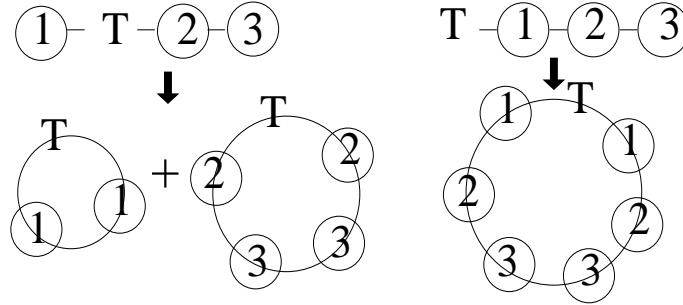


FIG. 18: Correspondence between a confining four-site 1D system with a deep trap T and periodic systems of different sizes for the two possible symmetry-distinct trap configurations. Sites with same numbers are symmetry-equivalent. In our model, the heavy walker 2 plays the role of the deep trap T in the figure. For $p = 0$ the system in the left subfigure will be equivalent to a three- (five-) site system if walker 1 starts to the left (right) of walker 2. Similarly, the system in the right subfigure will be equivalent to a seven-site periodic system. From this picture one can easily infer that the motion of the trap in the case $p > 0$ is associated with lattice size fluctuations in the periodic lattice representation.

APPENDIX A: TABLES WITH ANALYTIC RESULTS FOR THE GENERAL CASE IN 1D

N	$\langle n \rangle$
2	$2/(2p_1 + 2p_2 - 3p_1p_2)$
3	$2/(p_1 + p_2 - p_1p_2)$
4	$(10/3)(4p_1 + 4p_2 - 7p_1p_2)/(4p_1^2 + 8p_1p_2 - 10p_1^2p_2 + 4p_2^2 - 10p_1p_2^2 + 5p_1^2p_2^2)$
5	$(20p_1 + 20p_2 - 28p_1p_2)/((p_1p_2 - 2p_1 - 2p_2)(3p_1p_2 - 2p_1 - 2p_2))$
6	$(28/5)(-20p_1p_2 - 10p_1^2 + 30p_1^2p_2 - 10p_2^2 + 30p_1p_2^2 - 21p_1^2p_2^2)/(-24p_1^2p_2 - 24p_1p_2^2 + 56p_1^2p_2^2 - 8p_1^3 - 8p_2^3 + 28p_1^3p_2 - 28p_1^2p_2^2 + 28p_1p_2^3 - 28p_1^2p_2^3 + 7p_1^3p_2^3)$
7	$(-4/3)(21p_1^2p_2^2 - 36p_1^2p_2 + 14p_1^2 - 36p_1p_2^2 + 28p_1p_2 + 14p_2^2)/((p_1^2p_2^2 - 4p_1^2p_2 + 2p_1^2 - 4p_1p_2^2 + 4p_1p_2 + 2p_2^2)(-p_1 - p_2 + p_1p_2))$
8	$(12/7)(-231p_1^3p_2^3 + 594p_1^3p_2^2 - 462p_1^3p_2 + 112p_1^3 + 594p_1^2p_2^3 - 924p_1^2p_2^2 + 336p_1^2p_2 - 462p_1p_2^3 + 336p_1p_2^2 + 112p_2^3)/(3p_1^3p_2^3 - 18p_1^3p_2^2 + 24p_1^3p_2 - 8p_1^3 - 18p_1^2p_2^3 + 48p_1^2p_2^2 - 24p_1^2p_2 + 24p_1p_2^3 - 24p_1p_2^2 - 8p_2^3)(-2p_1 - 2p_2 + 3p_1p_2)$
9	$-10(33p_1^3p_2^3 - 99p_1^3p_2^2 + 88p_1^3p_2 - 24p_1^3 - 99p_1^2p_2^3 + 176p_1^2p_2^2 - 72p_1^2p_2 + 88p_1p_2^3 - 72p_1p_2^2 - 24p_2^3)/((p_1^2p_2^2 - 6p_1^2p_2 + 4p_1^2 - 6p_1p_2^2 + 8p_1p_2 + 4p_2^2)(4p_1^2 + 8p_1p_2 - 10p_1^2p_2 + 4p_2^2 - 10p_1p_2^2 + 5p_1^2p_2^2))$
10	$(-22/9)(429p_1^4p_2^4 - 1716p_1^3p_2^4 + 240p_2^4 + 2288p_1^2p_2^4 - 1248p_1p_2^4 - 1716p_1^4p_2^3 - 1248p_1^4p_2 + 240p_1^4 + 2288p_1^4p_2^2 - 3744p_1^2p_2^3 + 960p_1p_2^3 - 3744p_1^3p_2^2 + 960p_1^3p_2 + 1440p_1^2p_2^2 + 4576p_1^3p_2^3)/((11p_1^5p_2^5 - 110p_1^5p_2^4 + 308p_1^5p_2^3 - 352p_1^5p_2^2 + 176p_1^5p_2 - 32p_1^5 - 110p_1^4p_2^5 + 616p_1^4p_2^4 - 1056p_1^4p_2^3 + 704p_1^4p_2^2 - 160p_1^4p_2 + 308p_1^3p_2^5 - 1056p_1^3p_2^4 + 1056p_1^3p_2^3 - 320p_1^3p_2^2 - 352p_2^5p_1^2 + 704p_1^2p_2^4 - 320p_1^2p_2^3 + 176p_1p_2^5 - 160p_1p_2^4 - 32p_2^5))$

TABLE 10: *Polynomial expressions for $\langle n \rangle$ in the general case (1D periodic lattices of increasing size N).*

N	$p_{1,c}^{(n)}$
4	.833972
6	.902207
8	.936378
10	.955625
12	.967419

TABLE 11: Critical values $p_{1,c}^{(n)}$ (1D periodic lattices of increasing size N).

N	$\langle v \rangle$
2	$2(2 - 2p_1 - 2p_2 + 3p_1p_2)/(-2p_1 - 2p_2 + 3p_1p_2)^2$
3	$2(2 - p_1 - p_2 + p_1p_2)/(-p_1 - p_2 + p_1p_2)^2$
4	$(2/3)(272p_1^2 + 544p_1p_2 - 1200p_1p_2^2 + 1530p_1^2p_2^2 + 340p_1^3p_2 - 450p_1^3p_2^2 + 340p_2^3p_1 - 450p_1^2p_2^3 + 175p_1^3p_2^3 - 1200p_1^2p_2 - 80p_1^3 - 80p_2^3 + 272p_2^2)/(4p_1^2 + 8p_1p_2 - 10p_1^2p_2 + 4p_2^2 - 10p_1p_2^2 + 5p_1^2p_2^2)^2$
5	$4(21p_1^3p_2^3 - 71p_1^3p_2^2 + 68p_1^3p_2 - 20p_1^3 - 71p_1^2p_2^3 + 348p_1^2p_2^2 - 356p_1^2p_2 + 104p_1^2 + 68p_2^3p_1 - 356p_1p_2^2 + 208p_1p_2 - 20p_2^3 + 104p_2^2)/((p_1p_2 - 2p_1 - 2p_2)^2(-2p_1 - 2p_2 + 3p_1p_2)^2)$
6	$(28/5)(-3984p_1p_2^4 + 10056p_1^2p_2^4 - 80p_1^5 + 592p_2^4 - 11592p_1^4p_2^3 - 1288p_1^5p_2^2 + 1498p_1^5p_2^3 - 11592p_1^3p_2^4 + 5754p_1^4p_2^4 - 798p_1^5p_2^4 + 520p_1^5p_2 - 3984p_1^4p_2 + 10056p_1^4p_2^2 + 592p_1^4 + 3552p_1^2p_2^2 + 19072p_1^3p_2^3 - 11552p_1^3p_2^2 + 2368p_2^3p_1 - 11552p_1^2p_2^3 + 2368p_1^3p_2 + 1498p_1^3p_2^5 - 798p_1^4p_2^5 + 147p_1^5p_2^5 - 80p_2^5 + 520p_2^5p_1 - 1288p_2^5p_1^2)/(-24p_1^2p_2 - 24p_1p_2^2 + 56p_1^2p_2^2 + 7p_1^3p_2^3 - 28p_1^3p_2^2 + 28p_2^3p_1 - 28p_1^2p_2^3 + 28p_1^3p_2 - 8p_1^3 - 8p_2^3)^2$
7	$(4/3)(-1596p_1p_2^4 + 3384p_1^2p_2^4 - 28p_1^5 + 280p_2^4 - 3240p_1^4p_2^3 - 328p_1^5p_2^2 + 320p_1^5p_2^3 - 3240p_1^3p_2^4 + 1314p_1^4p_2^4 - 141p_1^5p_2^4 + 156p_1^5p_2 - 1596p_1^4p_2 + 3384p_1^4p_2^2 + 280p_1^4 + 1680p_1^2p_2^2 + 6456p_1^3p_2^3 - 4648p_1^3p_2^2 + 1120p_2^3p_1 - 4648p_1^2p_2^3 + 1120p_1^3p_2 + 320p_1^3p_2^5 - 141p_1^4p_2^5 + 21p_1^5p_2^5 - 28p_2^5 + 156p_2^5p_1 - 328p_2^5p_1^2)/((p_1^2p_2^2 - 4p_1^2p_2 + 2p_1^2 - 4p_1p_2^2 + 4p_1p_2 + 2p_2^2)^2(-p_1 - p_2 + p_1p_2)^2)$

TABLE 12: Polynomial expressions for $\langle v \rangle$ in the general case (1D periodic lattices of size $N = 2$ to $N = 7$).

N	$\langle v \rangle$
8	$ \begin{aligned} & (12/7)(349440p_1^2p_2^4 - 1998080p_1^4p_2^3 - 1005312p_1^5p_2^2 + 2845920p_1^5p_2^3 - 1998080p_1^3p_2^4 \\ & + 4230240p_1^4p_2^4 - 3982752p_1^5p_2^4 + 139776p_1^5p_2 + 349440p_1^4p_2^2 + 465920p_1^3p_2^3 - 54864p_2^7p_1^2 \\ & - 54864p_1^7p_2^2 + 64746p_1^5p_2^7 + 103080p_1^3p_2^7 - 19206p_1^7p_2^6 - 19206p_1^6p_2^7 + 2079p_1^7p_2^7 \\ & - 109512p_1^7p_2^4 + 64746p_1^7p_2^5 + 103080p_1^7p_2^3 - 109512p_1^4p_2^7 + 236610p_1^6p_2^6 - 867528p_1^5p_2^6 \\ & + 746256p_2^6p_1^2 - 1419024p_2^6p_1^3 + 1505928p_2^6p_1^4 - 867528p_1^6p_2^5 - 1419024p_1^6p_2^3 + 1505928p_1^6p_2^4 \\ & + 746256p_1^6p_2^2 + 23296p_2^6 + 15456p_1^7p_2 + 15456p_2^7p_1 - 1792p_1^7 + 23296p_1^6 - 206080p_1^6p_2 \\ & - 206080p_2^6p_1 + 2845920p_1^3p_2^5 - 3982752p_1^4p_2^5 + 2805696p_1^5p_2^5 + 139776p_2^5p_1 \\ & - 1005312p_2^5p_1^2 - 1792p_2^7)/((3p_1^3p_2^3 - 18p_1^3p_2^2 + 24p_1^3p_2 - 8p_1^3 - 18p_1^2p_2^3 + 48p_1^2p_2^2 \\ & - 24p_1^2p_2 + 24p_2^3p_1 - 24p_1p_2^2 - 8p_2^3)^2(-2p_1 - 2p_2 + 3p_1p_2)^2) \end{aligned} $
9	$ \begin{aligned} & 2(3000448p_1^5p_2^3 - 1203840p_1^5p_2^2 + 188928p_1^5p_2 - 3669728p_1^5p_2^4 + 3000448p_1^3p_2^5 - 1203840p_1^2p_2^5 \\ & + 188928p_1p_2^5 - 3669728p_1^4p_2^5 + 2238576p_1^5p_2^5 + 629760p_1^3p_2^3 + 472320p_1^4p_2^2 - 2394240p_1^4p_2^3 \\ & + 472320p_1^2p_2^4 - 2394240p_1^3p_2^4 + 4463872p_1^4p_2^4 + 825p_1^7p_2^7 + 783232p_1^6p_2^2 - 1300176p_1^6p_2^3 \\ & + 1195368p_1^6p_2^4 - 591060p_1^6p_2^5 - 70340p_1^4p_2^7 + 76080p_1^3p_2^7 - 46160p_1^2p_2^7 + 35860p_1^5p_2^7 \\ & - 9075p_1^6p_2^7 - 70340p_1^7p_2^4 + 76080p_1^7p_2^3 - 46160p_1^7p_2^2 + 35860p_1^7p_2^5 - 591060p_1^5p_2^6 + 1195368p_1^4p_2^6 \\ & - 1300176p_1^3p_2^6 + 136620p_1^6p_2^6 - 9075p_1^7p_2^6 + 14720p_1^7p_2 + 783232p_1^2p_2^6 + 14720p_1p_2^7 + 31488p_2^6 \\ & + 31488p_1^6 - 1920p_1^7 - 1920p_2^7 - 246144p_1^6p_2 - 246144p_1p_2^6)/((p_1^2p_2^2 - 6p_1p_2^2 + 4p_2^2 - 6p_1^2p_2 \\ & + 8p_1p_2 + 4p_1^2)^2(4p_2^2 + 8p_1p_2 - 10p_1p_2^2 + 4p_1^2 - 10p_1^2p_2 + 5p_1^2p_2^2)^2) \end{aligned} $
10	$ \begin{aligned} & (22/9)(8687616p_1^5p_2^3 - 57738240p_1^5p_2^4 + 8687616p_1^3p_2^5 - 57738240p_1^4p_2^5 + 150474240p_1^5p_2^5 \\ & - 97613824p_1^7p_2^4 + 10859520p_1^4p_2^4 + 1236378p_1^8p_2^8 + 37019488p_1^7p_2^7 + 20033904p_1^6p_2^8 \\ & - 7090512p_1^7p_2^8 + 155136p_2^8 - 20579328p_1^8p_2^3 + 32759936p_1^8p_2^4 - 32651520p_1^8p_2^5 - 1691136p_1^8p_2 \\ & + 20033904p_1^8p_2^6 - 7090512p_1^8p_2^7 + 7893504p_1^2p_2^8 - 20579328p_1^3p_2^8 + 32759936p_1^4p_2^8 - 32651520p_1^5p_2^8 \\ & - 1691136p_1p_2^8 + 7893504p_1^8p_2^2 + 4343808p_1^6p_2^2 - 34707456p_1^6p_2^3 + 113143296p_1^6p_2^4 - 192586240p_1^6p_2^5 \\ & + 155136p_1^8 - 97613824p_1^4p_2^7 + 45717504p_1^3p_2^7 - 11630592p_1^2p_2^7 + 122302400p_1^5p_2^7 - 90295040p_1^6p_2^7 \\ & + 45717504p_1^7p_2^3 - 11630592p_1^7p_2^2 + 122302400p_1^7p_2^5 - 192586240p_1^5p_2^6 + 113143296p_1^4p_2^6 \\ & - 34707456p_1^3p_2^6 + 181026560p_1^6p_2^6 - 90295040p_1^7p_2^6 + 1241088p_1^7p_2 + 1241088p_1p_2^7 + 4343808p_1^2p_2^6 \\ & - 7680p_1^9 - 7680p_2^9 - 1531904p_1^9p_2^4 + 1524160p_1^9p_2^5 - 944944p_1^9p_2^6 + 346060p_1^9p_2^7 + 970816p_1^9p_2^3 \\ & - 377344p_1^9p_2^2 + 82176p_1^9p_2 - 66066p_1^9p_2^8 - 1531904p_1^4p_2^9 + 1524160p_1^5p_2^9 - 944944p_1^6p_2^9 \\ & + 346060p_1^7p_2^9 + 970816p_1^3p_2^9 - 377344p_1^2p_2^9 + 82176p_1p_2^9 - 66066p_1^8p_2^9 + 4719p_1^9p_2^9)/(11p_1^5p_2^5 \\ & - 110p_1^4p_2^5 + 308p_1^3p_2^5 - 352p_1^2p_2^5 + 176p_1p_2^5 - 32p_2^5 - 110p_1^5p_2^4 + 616p_1^4p_2^4 - 1056p_1^3p_2^4 \\ & + 704p_1^2p_2^4 - 160p_1p_2^4 + 308p_1^5p_2^3 - 1056p_1^4p_2^3 + 1056p_1^3p_2^3 - 320p_1^2p_2^3 - 352p_1^5p_2^2 \\ & + 704p_1^4p_2^2 - 320p_1^3p_2^2 + 176p_1^5p_2 - 160p_1^4p_2 - 32p_1^5)^2 \end{aligned} $

TABLE 13: Polynomial expressions for $\langle v \rangle$ in the general case (1D periodic lattices of size $N = 7$ to $N = 10$).

N	$p_{1,c}^{(v)}$
4	.817442
6	.891104
8	.929001
10	.950475

TABLE 14: *Critical values $p_{1,c}^{(v)}$ (1D periodic lattices of increasing size).*

APPENDIX B: TABLES WITH ANALYTIC RESULTS FOR THE GENERAL CASE IN 2D

N	$\langle n \rangle$
4	$-(2/3)(71p_1p_2 - 40p_2 - 40p_1)/(13p_1^2p_2^2 - 22p_1p_2^2 - 22p_1^2p_2 + 8p_2^2 + 16p_1p_2 + 8p_1^2)$
9	$-8(11p_1p_2 - 9p_1 - 9p_2)/(7p_1^2p_2^2 - 16p_1^2p_2 - 16p_1p_2^2 + 8p_1^2 + 16p_1p_2 + 8p_2^2)$
16	$-(8/45)(26497p_1^3p_2^3 - 68308p_1^3p_2^2 + 53804p_1^3p_2 - 13184p_1^3 - 68308p_1^2p_2^3 + 107608p_1^2p_2^2 - 39552p_1^2p_2 + 53804p_1p_2^3 - 39552p_1p_2^2 - 13184p_2^3)/(147p_1^4p_2^4 - 664p_1^4p_2^3 + 1000p_1^4p_2^2 - 608p_1^4p_2 + 128p_1^4 - 664p_1^3p_2^4 + 2000p_1^3p_2^3 - 1824p_1^3p_2^2 + 512p_1^3p_2 + 1000p_1^2p_2^4 - 1824p_1^2p_2^3 + 768p_1^2p_2^2 - 608p_1p_2^4 + 512p_1p_2^3 + 128p_2^4)$
25	$-(76/3)(1920p_1^2p_2^2 - 3984p_1^3p_2^2 + 1280p_1^3p_2 - 1185p_1^3p_2^4 - 1185p_1^4p_2^3 + 1940p_1^4p_2^2 + 1940p_1^2p_2^4 + 1280p_1p_2^3 + 3880p_1^3p_2^3 - 3984p_1^2p_2^3 - 1328p_1^4p_2 + 320p_2^4 + 255p_1^4p_2^4 - 1328p_1^4p_2 + 320p_1^4)/(95p_1^5p_2^5 - 684p_1^5p_2^4 - 2560p_1^3p_2^2 + 1788p_1^5p_2^3 - 2160p_1^5p_2^2 + 1216p_1^5p_2 - 256p_1^5 - 684p_1^4p_2^5 + 3576p_1^4p_2^4 - 6480p_1^4p_2^3 + 4864p_1^4p_2^2 - 1280p_1^4p_2 + 1788p_1^3p_2^5 - 6480p_1^3p_2^4 + 7296p_1^3p_2^3 - 2160p_1^2p_2^5 + 4864p_1^2p_2^4 - 2560p_1^2p_2^3 + 1216p_1p_2^5 - 1280p_2^4p_1 - 256p_2^5)$
36	$-(2/1225)(-12930686208p_1^7p_2^4 - 12930686208p_1^4p_2^7 + 15328776360p_1^6p_2^6 - 38792058624p_1^5p_2^5 - 5200699392p_1^5p_2^2 - 5200699392p_2^5p_1^2 + 74710699776p_1^5p_2^5 + 30453427200p_1^5p_2^3 - 68813798400p_1^4p_2^5 + 30453427200p_1^3p_2^5 + 49807133184p_1^6p_2^4 - 38792058624p_1^6p_2^5 - 34406899200p_1^6p_2^3 + 49807133184p_1^4p_2^6 - 34406899200p_1^3p_2^6 + 12181370880p_1^6p_2^6 - 68813798400p_1^5p_2^4 - 1733566464p_1^6p_2 - 1733566464p_1p_2^6 + 12181370880p_1^6p_2^2 + 40604569600p_1^4p_2^4 - 8667832320p_1^3p_2^4 - 8667832320p_1^4p_2^3 + 298340359p_1^7p_2^7 - 2385516420p_1^7p_2^6 - 2385516420p_1^6p_2^7 + 7664388180p_1^7p_2^5 + 7664388180p_1^5p_2^7 - 247652352p_2^7 + 12451783296p_1^3p_2^7 - 6881379840p_1^2p_2^7 + 2030228480p_1p_2^7 - 247652352p_1^7 + 12451783296p_1^7p_2^3 - 6881379840p_1^7p_2^2 + 2030228480p_1^7p_2)/(193480p_2^8p_1^6 - 71680p_1p_2^8 - 530176p_1^3p_2^8 + 263680p_1^2p_2^8 - 457880p_1^5p_2^8 + 633728p_1^4p_2^8 - 71680p_1^8p_2 - 2650880p_1^7p_2^4 - 457880p_1^8p_2^5 - 530176p_1^8p_2^3 + 263680p_1^8p_2^2 + 633728p_1^8p_2^4 - 2650880p_1^4p_2^7 + 3802368p_1^6p_2^6 - 5301760p_1^6p_2^5 - 5301760p_1^5p_2^6 + 5273600p_1^5p_2^5 - 2508800p_1^5p_2^4 + 458752p_1^5p_2^3 - 2508800p_1^4p_2^5 + 458752p_1^3p_2^5 + 3955200p_1^6p_2^4 - 1505280p_1^6p_2^3 + 3955200p_1^4p_2^6 - 1505280p_1^3p_2^6 + 229376p_1^2p_2^6 + 229376p_1^6p_2^2 + 573440p_1^4p_2^4 + 193480p_1^8p_2^6 + 8192p_1^8 + 386960p_1^7p_2^7 - 1373640p_1^7p_2^6 - 1373640p_1^6p_2^7 + 2534912p_1^7p_2^5 + 2534912p_1^5p_2^7 + 3815p_1^8p_2^8 - 43154p_1^8p_2^7 - 43154p_1^7p_2^8 + 8192p_2^8 + 1582080p_1^3p_2^7 - 501760p_1^2p_2^7 + 65536p_1p_2^7 + 1582080p_1^7p_2^3 - 501760p_1^7p_2^2 + 65536p_1^7p_2)$

TABLE 15: Polynomial expressions for $\langle n \rangle$ in the general case (2D periodic square planar lattices of increasing size)

N	$p_{1,c}^{(n)}$
4	.710835
16	.842153
36	.887094

TABLE 16: Critical values $p_{1,c}^{(n)}$ (2D square planar lattices of increasing size with an even value of N).

N	$\langle v \rangle$
4	$(2/3)(2176p_1p_2 - 2082p_1^2p_2^3 + 923p_1^3p_2^3 - 2082p_1^3p_2^2 + 1448p_2^3p_1 + 1448p_1^3p_2 - 320p_1^3 - 320p_2^3 + 1088p_1^2 - 4864p_1^2p_2 + 1088p_2^2 - 4864p_1p_2^2 + 6418p_1^2p_2^2)/(13p_1^2p_2^2 - 22p_1p_2^2 + 8p_2^2 - 22p_1^2p_2 + 16p_1p_2 + 8p_1^2)^2$
9	$8(1312p_1p_2 - 239p_1^2p_2^3 + 77p_1^3p_2^3 - 239p_1^3p_2^2 + 232p_2^3p_1 + 232p_1^3p_2 - 72p_1^3 - 72p_2^3 + 656p_1^2 - 1832p_1^2p_2 + 656p_2^2 - 1832p_1p_2^2 + 1464p_1^2p_2^2)/(-16p_1^2p_2 - 16p_1p_2^2 + 7p_1^2p_2^2 + 8p_1^2 + 16p_1p_2 + 8p_2^2)^2$
16	$(8/135)(44708352p_1^7p_2 + 44708352p_2^7p_1 + 1879900160p_1^3p_2^3 + 1409925120p_1^4p_2^2 - 7866368000p_1^4p_2^3 + 1409925120p_2^4p_1^3 - 7866368000p_1^3p_2^4 + 16208510208p_1^4p_2^4 - 3950903296p_1^2p_2^5 - 5062656p_1^7 + 10880187392p_1^3p_2^5 - 14811384576p_1^4p_2^5 + 10880187392p_1^5p_2^3 - 14811384576p_1^5p_2^4 + 10174354048p_1^5p_2^5 + 563970048p_2^5p_1 + 563970048p_1^5p_2 + 93995008p_1^6 + 93995008p_2^6 - 5062656p_2^7 - 3094999904p_1^5p_2^6 + 5409620192p_1^4p_2^6 - 5210329472p_1^3p_2^6 + 2820640640p_1^2p_2^6 + 869041300p_1^6p_2^6 - 3094999904p_1^6p_2^5 + 5409620192p_1^6p_2^4 - 5210329472p_1^6p_2^3 + 2820640640p_1^6p_2^2 - 804356096p_2^6p_1 - 804356096p_1^6p_2 - 366246240p_1^4p_2^7 + 239288100p_1^5p_2^7 - 82905852p_1^6p_2^7 - 82905852p_1^7p_2^6 + 11685177p_1^7p_2^7 + 239288100p_1^7p_2^5 - 366246240p_1^7p_2^4 + 322443168p_2^7p_1^3 - 3950903296p_1^5p_2^2 + 322443168p_2^3p_1^7 - 163920768p_1^7p_2^2 - 163920768p_2^7p_1^2)/(147p_1^4p_2^4 - 664p_1^3p_2^4 + 1000p_2^4p_1^2 - 608p_2^4p_1 + 128p_2^4 - 664p_1^4p_2^3 + 2000p_1^3p_2^3 - 1824p_1^2p_2^3 + 512p_2^3p_1 + 1000p_1^4p_2^2 - 1824p_1^3p_2^2 + 768p_1^2p_2^2 - 608p_1^4p_2 + 512p_1^3p_2 + 128p_1^4)^2$

TABLE 17: Polynomial expressions for $\langle v \rangle$ in the general case (2D periodic square planar lattices of increasing size)

N	$p_{1,c}^{(v)}$
4	.702484
16	.837365
36	.885175

TABLE 18: Critical values $p_{1,c}^{(v)}$ (2D periodic square planar lattices of increasing size with an even number of sites N).